ESC European Society of Cardiology

European Heart Journal - Cardiovascular Imaging (2022) **23**, 867–884
https://doi.org/10.1093/ehjci/jeac011

REVIEW

Imaging assessment of the right atrium: anatomy and function

Roberto M. Lang[1]*, Matteo Cameli[2], L. Elif Sade[3,4], Francesco F. Faletra[5], Federico Fortuni [6,7], Alexia Rossi[8,9], and Laurie Soulat-Dufour[10]

[1]Heart and Vascular Center, University of Chicago, 5758 S Maryland Avenue, MC 9067, DCAM 5509, Chicago, IL 60637, USA; [2]Division of Cardiology, Department of Medical Biotechnologies, University of Siena, Siena, Italy; [3]University of Pittsburgh Medical Center, Heart and Vascular Institute, Pittsburgh, PA, USA; [4]Department of Cardiology, University of Baskent, Ankara, Turkey; [5]Division of Cardiology, Fondazione Cardiocentro Ticino, Lugano, Switzerland; [6]Department of Cardiology, San Giovanni Battista Hospital, Foligno, Italy; [7]Department of Cardiology, Leiden University Medical Center, Leiden, The Netherlands; [8]Department of Nuclear Medicine, Zurich University Hospital, Zurich, Switzerland; [9]Center for Molecular Cardiology, University of Zurich, Schlieren, Zurich, Switzerland; and [10]Saint Antoine and Tenon Hospital, AP-HP, Pr Ariel Cohen, Sorbonne Université, INSERM, Unité de recherche sur les maladies cardiovasculaires, le métabolisme et la nutrition, ICAN, Paris F-75013, France

Received 15 November 2021; editorial decision 10 January 2022; accepted 12 January 2022; online publish-ahead-of-print 25 January 2022

The right atrium (RA) is the cardiac chamber that has been least well studied. Due to recent advances in interventional cardiology, the need for greater understanding of the RA anatomy and physiology has garnered significant attention. In this article, we review how a comprehensive assessment of RA dimensions and function using either echocardiography, cardiac computed tomography, and magnetic resonance imaging may be used as a first step towards a better understanding of RA pathophysiology. The recently published normative data on RA size and function will likely shed light on RA atrial remodelling in atrial fibrillation (AF), which is a complex phenomenon that occurs in both atria but has only been studied in depth in the left atrium. Changes in RA structure and function have prognostic implications in pulmonary hypertension (PH), where the increased right ventricular (RV) afterload first induces RV remodelling, predominantly characterized by hypertrophy. As PH progresses, RV dysfunction and dilatation may begin and eventually lead to RV failure. Thereafter, RV overload and increased RV stiffness may lead to a proportional increase in RA pressure. This manuscript provides an in-depth review of RA anatomy, function, and haemodynamics with particular emphasis on the changes in structure and function that occur in AF, tricuspid regurgitation, and PH.

Keywords right atrium • echocardiography • computed tomography • magnetic resonance imaging • atrial fibrillation • pulmonary hypertension

Due to recent advances in interventional cardiology, the need for a greater understanding of right atrial (RA) anatomy has garnered significant attention. In fact, the RA and the interatrial septum serve not just as direct targets of interventions, such as transcatheter ablation of the cavo-tricuspid isthmus (CVTI) but also as the entry gate to access left heart chambers for a wide array of complex electrophysiology and structural heart interventions. Thus, optimal outcomes of intracardiac procedures mandate an excellent knowledge of RA anatomy, including recognition of common variants (*Table 1*).

The normal RA shows an ellipsoid shape, it is located superior to the right ventricle (RV), and anterior and lateral to the left atrium. It consists of a venous component, an appendage, and a vestibule.[1] The RA receives venous blood from the superior (SVC) and inferior (IVC) cava veins, the coronary sinus, and the Thebesian veins that drain the myocardium. During cardiac catheterization, the SVC is often the preferred site of entry into the RA. The SVC inserts upon the RA superior wall, with a mean mediolateral diameter of 20 ± 3 mm and a anteroposterior diameter of 19 ± 3 mm.[2]

Anatomically, the RA (*Figures 1 and 2*) includes five key structures: (i) crista terminalis (CT), (ii) RA appendage (RAA), (iii) CVTI, (iv) Eustachian valve (EV), and (v) orifice of coronary sinus and Thebesian valve.[1,2,4] The CT (*Figures 1 and 2*) is a muscular band which arises from the RA anteromedial wall, extending vertically along the SVC and IVC, with a mean length and thickness of 51 ± 9 mm and 5.5 mm, respectively.[5] On occasion, the CT can be quite prominent, thereby raising clinical concern for an RA mass (pseudo-mass, tumour, thrombus, or vegetation). Due to the non-uniformity of the myocardial fibre arrangements within and outside the CT, this region is the electroanatomic focus of up to two-thirds of focal RA tachycardia cases[2,6] (*Table 1*).

*Corresponding author. Tel: +1 773 702 1842; Fax: +1 773 702 1034. E-mail: rlang@medicine.bsd.uchicago.edu

The RAA (*Figures 1 and 2*) is derived from the 'embryological' RA, generally exhibiting a triangular shape, and forming most of the anterior and lateral RA walls. Typically, an extensive array of pectinate muscles spreads perpendicularly or obliquely from the CT, lining the internal surface of the RAA, resulting in a characteristic 'corrugated' surface appearance. Between pectinate muscles, the atrial wall may be very thin, comprising of only a few layers of myocytes between the epicardium and endocardium. One prominent pectinate muscle, the sagittal bundle, crosses the RAA wall transversely, dividing the RAA into the anteromedial and posterolateral portion. This large pectinate muscle (12 mm × 0.4 mm) is solitary in 55–65%, numerous (>1) in 20–25%, and absent in 15–20% of human hearts.[7]

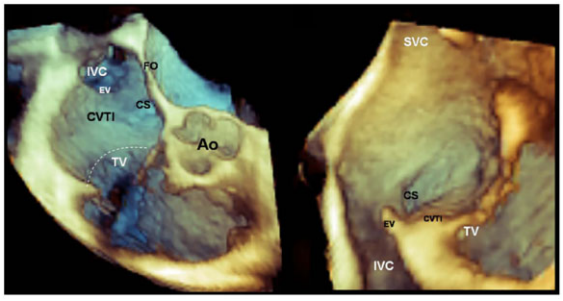

Figure 1 Three-dimensional anatomy of the right atrium. CVTI, crista terminalis; EV, Eustachian valve; CS, Coronary sinus; IVC, inferior vena cava; SVC, superior vena cava; TV, tricuspid valve; AO, aortic valve; FO, fossa ovalis. Modified from Ref.[3]

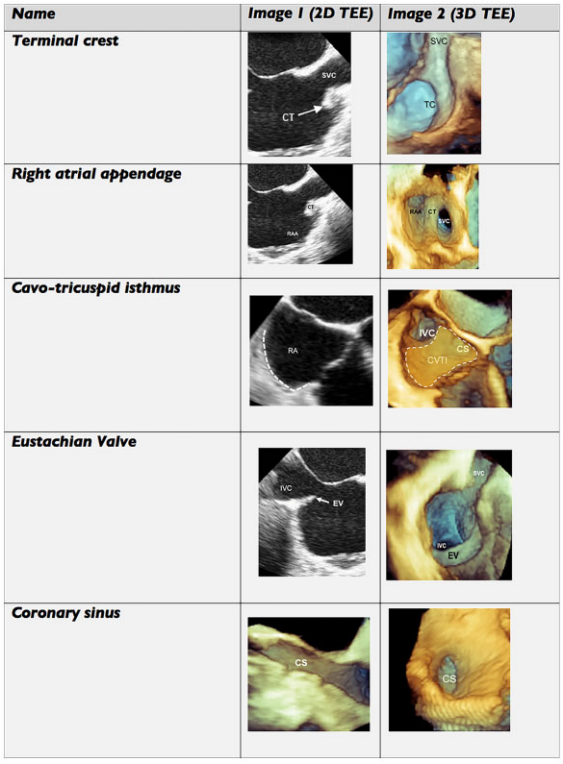

Figure 2 Two- and three-dimensional echocardiographic images of the crista terminalis, right atrial appendage, cavo-tricuspid isthmus, Eustachian valve, and coronary sinus.

The presence of a highly trabeculated appendage can herald challenges in transcatheter ablation cases. Anteriorly, the RAA ends with a pouch-like structure, which provides a stable position for implanting leads, reducing the risk of dislodgment. The junction between RAA and the RA is larger than the left atrial appendage orifice, which facilitates a more favourable 'washing out' of blood flow. This anatomical consideration likely explains the observation that formation of thrombi is less common in the RAA when compared with the left counterpart (*Table 1*).

The orifice of the IVC (*Figures 1 and 2*) is rounded and located in the RA posteroinferior region; its mean diameters are 24 ± 6 mm and mean area = 4.8 ± 2 cm^2. The EV, a remnant of the embryonic right valve of the sinus venosus, arises from the anterior border of the IVC orifice. In foetal life, the EV serves a critical role in channelling umbilical oxygenated blood from the IVC across the fossa ovalis to the systemic circulation. Following birth, the EV does not appear to have any physiological role, and with adulthood frequently regresses into a thin flap. Failure of reabsorption of the foetal EV may result in a redundant, mobile membrane that partly covers the IVC orifice, with the potential for complications during interventional procedures. If an substantial residual EV is present, the use of SVC access is suggested.[8] In contrast, an incomplete, spot-like reabsorption may result in a mesh of thin filaments known as a Chiari network, which is present in ∼4.6% of the population, and is often found located close to the IVC orifice and the coronary sinus orifice. This structure is easily detectable by transthoracic echocardiography as a highly mobile and reflective structure.[9] Notably, this structure may prevent a catheter from advancing freely into the atrium and limiting the range of the catheter manipulation.

The Eustachian ridge (26 ± 4 mm × 2 ± 2 mm) is an extension of the EV, which continues towards the central fibrous body, above the coronary sinus ostium. Excessive thickening of the Eustachian ridge is present in 47.9% of the hearts and may cause complete conduction block during atrial flutter, requiring total ridge ablation[10] (*Figure 2*).

The coronary sinus (9–15 mm) drains into the posteromedial aspect of the RA, between the IVC and the right atrioventricular ostium (*Figure 2*). The coronary sinus (*Figure 1*) is used as a passage to the left heart epicardium during cardiac resynchronization therapy, catheter ablation of cardiac arrhythmias, defibrillation, and mitral valve annuloplasty.[11] An abnormally large diameter of the coronary sinus is an established risk factor for AV nodal re-entrant tachycardia. In nearly 80% of cases, its orifice is adjacent to the Thebesian valve. The shape of this valve varies from a clear crescentic flap (with or without fenestrations) to a thin strand-like, nearly invisible structure. Occasionally, an extensive imperforate flap over the ostium of the coronary sinus may make its cannulation challenging[12] (*Table 1*). If an obstructive Thebesian valve is detected by cardiac imaging prior to an intervention, access strategy to the coronary sinus should be modified. Radiofrequency energy has been used to perforate the Thebesian valve.

The CVTI is a quadrilateral-shaped, concave region demarcated anteriorly by the septal tricuspid leaflet attachment, and posteriorly by the EV. The CVTI is the prime target for ablation

Table 1 Important anatomic right atrial structures and their main anatomic variants that may represent issues for interventional cardiology

	Imaging tips	Tricks for interventional cardiology
SVC		– Preferred access to RA
Crista terminalis		– Conduction in the cavotricuspid isthmus courses preferentially along thicker bundles → punctual ablation of distal terminal crest ramification may result in the interruption of pathological conduction – also used as ablation target in patients with inappropriate sinus tachycardia
RA appendage	Study of RA appendage with TOE before intervention	Presence of prominent trabeculations: – May lead to abnormal propagation of excitatory impulses and predispose to re-entry circuits, resulting in severe atrial arrhythmias – provides higher risk of perforation of the atrial wall and of thrombus formation during radiofrequency catheter ablation
Sinus node		Main anatomic difficulties of sinus node ablation: – extensive location – close proximity to crista terminalis – cooling effects of the nodal artery
IVC ostium and Eustachian valve	TOE before procedure or intracardiac echography during the procedure	– Prominent Eustachian valve covering the whole IVC orifice (1.8%) directs the catheter towards RA superior part, → challenging catheterization of the RA and RV. – giant Eustachian valve (rare) → obstruction of the IVC or the formation of a thrombus → obstacle during transcatheter occlusion of PFO – prominent Eustachian ridge → obstacle for a catheter heading towards the CSO and cavotricuspid isthmus → may generate a line of fixed conduction block during typical atrial flutter (block of paraseptal isthmus can be achieved only after complete ridge ablation)
Coronary sinus	Perform either: – Cardiac CT before the procedure – or intracardiac echocardiography or left coronary angiography with levophase before the CSO cannulation	Elements leading to unsuccessful cannulation: – small CSO – anatomic barriers – Thebesian valve covering the ostium → particularly 'fold' types especially prone to CSO obstruction during procedures
Cavotricuspid isthmus	Before ablation: preferably by echocardiography: TTE, TOE, ++3D TTE (en-face view); or by CT/CMR	Cavotricuspid atrial flutter ablation: – paraseptal isthmus should be avoided → may lead to complete AV block (the thickness of the muscular layer in this region raises the amount of energy required for ablation, posing a greater risk of AV node injury) – central isthmus: presence of the sub-Eustachian recess prolongs ablation time and increases the complication risk; location near right coronary artery (2–11 mm) – intertrabecular recesses (25.0%), trabecular bridges (12.9%), and sub-Eustachian recesses make ablation more challenging
Koch's triangle	Assess Koch's triangle dimensions if it is not the target of the ablation procedure	– AV node ablation: base of Koch's triangle is the site for the 'slow pathway' of AVNRT, inferior paraseptal, septal, and superior paraseptal accessory pathways and other arrhythmias deriving from that location – Cavotricuspid ablation: risk of ablation of AV node in case of unknown Koch's triangle dimensions

Continued

Table 1 *Continued*

	Imaging tips	Tricks for interventional cardiology
Interatrial septum	TOE assistance for transeptal puncture minimizes intraprocedural complications (++3D if available): – Visualize LAA in search of a thrombus – accurate visualization of left and right surfaces of the interatrial septum (bicaval view)	Fossa ovalis types: – 'smooth' fossa ovalis (56%) – PFO channel (25%), present in about 10–35% of the general population and associated with cardioembolic stroke due to paradoxical embolization and/or in situ thrombus formation within the PFO channel on the left side of the septum – right-sided septal pouch (11%) which is a diverticulum within the atrial septum that may be associated with thrombus formation and ischemic stroke; left-sided septal pouch may be a trigger with increased risk of atrial fibrillation
	Pre-procedural imaging by CT/CMR to assess RA morphology is suggested	– net-like formation within the fossa ovalis (7%)

AV, atrioventricular; AVNRT, atrioventricular node reentrant tachycardia; CMR, cardiac magnetic resonance; CSO, coronary sinus ostium; CT, computed tomography; IVC, inferior vena cava; LAA, left atrial appendage; PFO, patent foramen ovale; RA, right atrial; SVC, superior vena cava; TOE, transoesophageal echocardiography; TTE, transthoracic echocardiography.

in an effort to interrupt the macro-re-entrant circuit of atrial flutter[13] (*Table 1*).

The triangle of Koch, situated in the vestibule of the RA, is the key anatomic landmark in localizing the AV node. While the individual size of this landmark may be highly variable between individuals, general knowledge of the triangle of Koch dimensions is crucial when performing radio-frequency catheter ablation to avoid unintentional ablation of the atrioventricular node and subsequent complete heart block (*Table 1*).[14]

The interatrial septum and the fossa ovalis are two overlapping RA anatomic components (*Figure 3*). The interatrial septum is defined as the fibro-muscular area interposed between both atria. Two common phenotypic variants are the presence of a 'lipomatous' septum or a large septal aneurysm, both of which can be easily visualized by 2D echocardiography. The fossa ovalis is an oval/round concave region of 14 ± 4 mm × 12 ± 4 mm located in the infero-posterior aspect of the interatrial septum composed mainly of thin fibrous tissue. The fossa area (143 ± 65 mm^2) typically enlarges with age. There are four variations of fossa ovalis anatomy as visualized from the RA perspective (*Table 1*).

RA morphology should be assessed prior to any interventional procedure involving a transseptal approach. Both cardiac computed tomography (CCT) and cardiac magnetic resonance (CMR) may adequately demonstrate the atrial septal anatomy prior to procedures; however, for both pre- and intra-procedural assistance, transoesophageal echocardiography (TOE) is the modality of choice (*Figure 3*). Specifically, 3D TOE may be used to generate an 'en-face' view of the interatrial septum, in real-time during interventions as guidance to optimize the site of transseptal puncture, and monitor thereafter. Given the feasibility, low cost, and real-time imaging characteristic, TOE remains the imaging modality of preference for interatrial septal assessment in most clinical settings.

RA size and function measured using echocardiography, CMR, and CT

A comprehensive assessment of RA dimensions and function using either echocardiography, CCT, or CMR acts as a first step towards a better understanding of its pathophysiology. The function of the RA is complex and can be divided into three phases: (i) a reservoir phase, during which it acts as reservoir for the vena caval blood returning during ventricular systole (atrial filling); (ii) a conduit phase, during passive RA emptying into the RV; and (iii) booster pump, during atrial contraction, that augments RV filling during late ventricular diastole[15] (*Figures 4 and 5B*).

Sex, age, and ethnic differences in RA size and function

Previous studies have reported sex differences in RA size, with larger RA volumes noted in men when using both 2D[16–20] and 3D[16,20] echocardiography even after body surface area (BSA) indexing. Conversely, RA function parameters (3D emptying fractions, strain) have been shown to be higher in women.[16,20]

With ageing, end-systolic RA volumes seem to remain stable by both 2D[18,20] and 3D echocardiography,[16] or even decrease slightly.[20] In contrast, both 3D end-diastolic volumes and 3D pre-A RA volumes enlarge with age.[16,20] Also, 3D RA total emptying fraction as well as reservoir strain, passive emptying fraction, and conduit strain

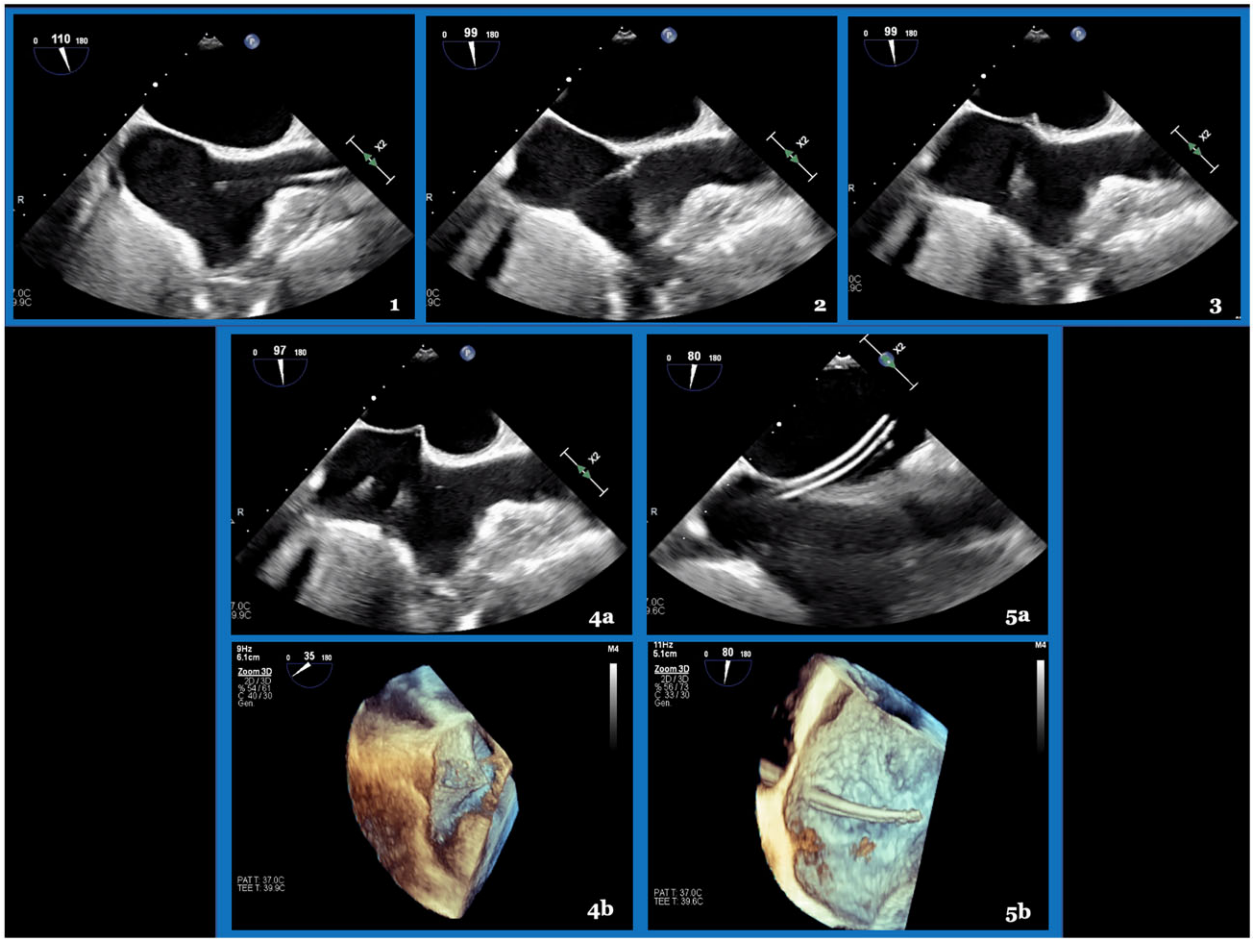

Figure 3 Transeptal puncture with bidimensional and tridimensional transesophageal echocardiographic assistance. From the bicaval view, the transeptal needle is initially positioned in the lower part of superior vena cava (*Panel 1*), then, is slowly pulled down (*Panel 2*) until it reaches the true fossa ovalis (*Panel 3*); in this position, the position of the needle is slightly adjusted until tenting is visualized (*Panel 4A* and *4B*). Then, after achieving the ideal position of the needle, the transeptal needle is advanced until passing through the interatrial septum to the left atrium (*Panel 5A* and *5B*).

magnitude decrease with age, whereas the magnitude of RA contractile strain increases.[16,20] Inter-vendor variability is likely responsible for some of the observed variability in RA strain normal values.[21] Other factors known to impact RA size and function include strenuous athletic activity[22] and body mass index.[23]

Until recently, most datasets informing normative RA size ranges, including those as published in the current guidelines[24] were primarily derived from White North American and European populations. This was somewhat problematic, as there was evidence to demonstrate that normal values for cardiac chambers differ by country and/or ethnicity, and accordingly, recent studies of large international cohorts were conducted to elucidate these differences.[25–27] Contemporary data from the World Alliance Societies of Echocardiography (WASE) study noted geographic differences in RA size.[20] Interestingly, Asians were found to have significantly smaller RA dimensions (both longitudinal and transverse) and RA volumes (both 2D and 3D end-systolic RA volumes), compared to non-Asians, even when adjusted for BSA. These results underscore the need for established normal values for RA size and volumes according to ethnicity.

Echocardiographic measurements of RA size and function

Results from several key echocardiographic studies examining techniques for RA size and function in populations of healthy individuals are listed in *Table 2*. Using 2D echocardiography, RA linear dimensions, areas, and volumes should be assessed from the apical four-chamber view[24] (*Figure 5B*). The minor-axis dimension should be measured from a plane perpendicular to the long axis of the RA, extending from the lateral border of the RA to the interatrial septum. RA volume is determined from this single-view using the area–length method and/or method of disks summation.[16,28,32–34] Studies have demonstrated that RA volumes obtained using the area–length method are slightly larger than those obtained using the method of disks summation.[9,17,18,35]

To avoid foreshortening of the RA chamber, a dedicated RA-focused view should be utilized for measurement of RA areas, volumes, and strain.[36] The recent development of specific 3D echocardiography software dedicated to quantifying the atria has improved the accuracy and feasibility of these measurements.[37]

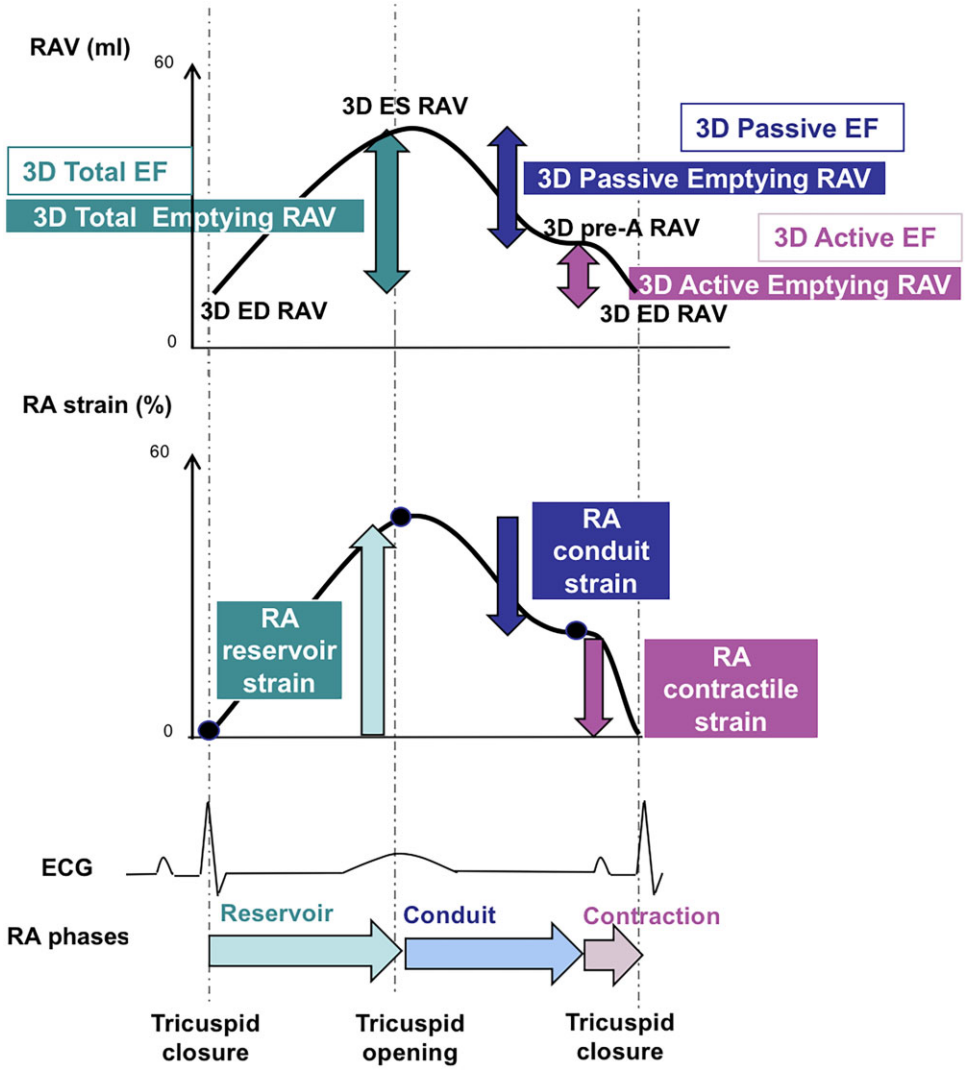

Figure 4 Physiology of the RA with the analysis of the RA volume curve (left) and the RA deformation (right). 3D total emptying RAV = (3D ES RAV) - (3D ED RAV); 3D passive emptying RAV = (3D ES RAV) - (3D pre-A RAV); 3D active emptying RAV = (3D pre-A RAV) - (3D ED RAV); 3D total EmF = (3D total emptying RAV)/(3D ES RAV); 3D passive EmF = (3D passive emptying RAV)/(3D ES RAV); 3D active EmF (atrial contraction) = (3D active emptying RAV)/(3D pre-A RAV). ED, end-diastolic; ES, end-systolic; pre-A, before atrial contraction; RA, right atrium/atrial; RAV, right atrial volume; EF, emptying fraction; ECG, electrocardiogram.

2D echocardiography

In the current echocardiographic guidelines issued by the American Society of Echocardiography (ASE) and European Association of Cardiovascular imaging (EACVI),[24] the normal values (mean ± standard deviation, or SD) of the indexed 2D RA major axis dimensions are 24 ± 3 mm/m^2 and 25 ± 3 mm/m^2 for men and women, respectively. For BSA-indexed 2D RA minor axis, the mean value is 19 ± 3 cm/m^2 for both sexes.[24,30] The reported normal values of the indexed 2D end-systolic RA volume (by area–length method) is 25 ± 7 mL/m^2 and 21 ± 6 mL/m^2 for men and women, respectively.[16,18,24] Studies using the single-plane method of disks have reported lower values for indexed 2D end-systolic RA volume. For example, in a large European multicentre study,[18] 22.5 ± 6.5 mL/m^2 and 19.0 ± 6.2 mL/m^2 were reported for men and women, respectively. Similarly, in a large worldwide study,[20] 20.6 ± 6.4 mL/m^2 and 18.0 ± 5.3 mL/m^2 were reported for men and women, respectively.

3D echocardiography

No partition values of 3D RA volumes are reported in the current ASE/EACVI guidelines.[24] However, recently, 3D RA volumes were found to be larger than their corresponding 2D RA volumes.[16,20] In 200 healthy European subjects, the mean/SD indexed 3D end-systolic RA volume was reported to be 31 ± 8 mL/m^2 for men and 27 ± 8 mL/m^2 for women.[16] In a large multicentre international cohort, the indexed 3D end-systolic RA volume was 23.2 ± 7.4 mL/m^2 for men and 20.5 ± 6.4 mL/m^2 for women.[20] No definitive normal values for RA function using either 2D or 3D are available in the current ASE/EACVI guidelines.[24] In single-centre studies, RA reservoir strain

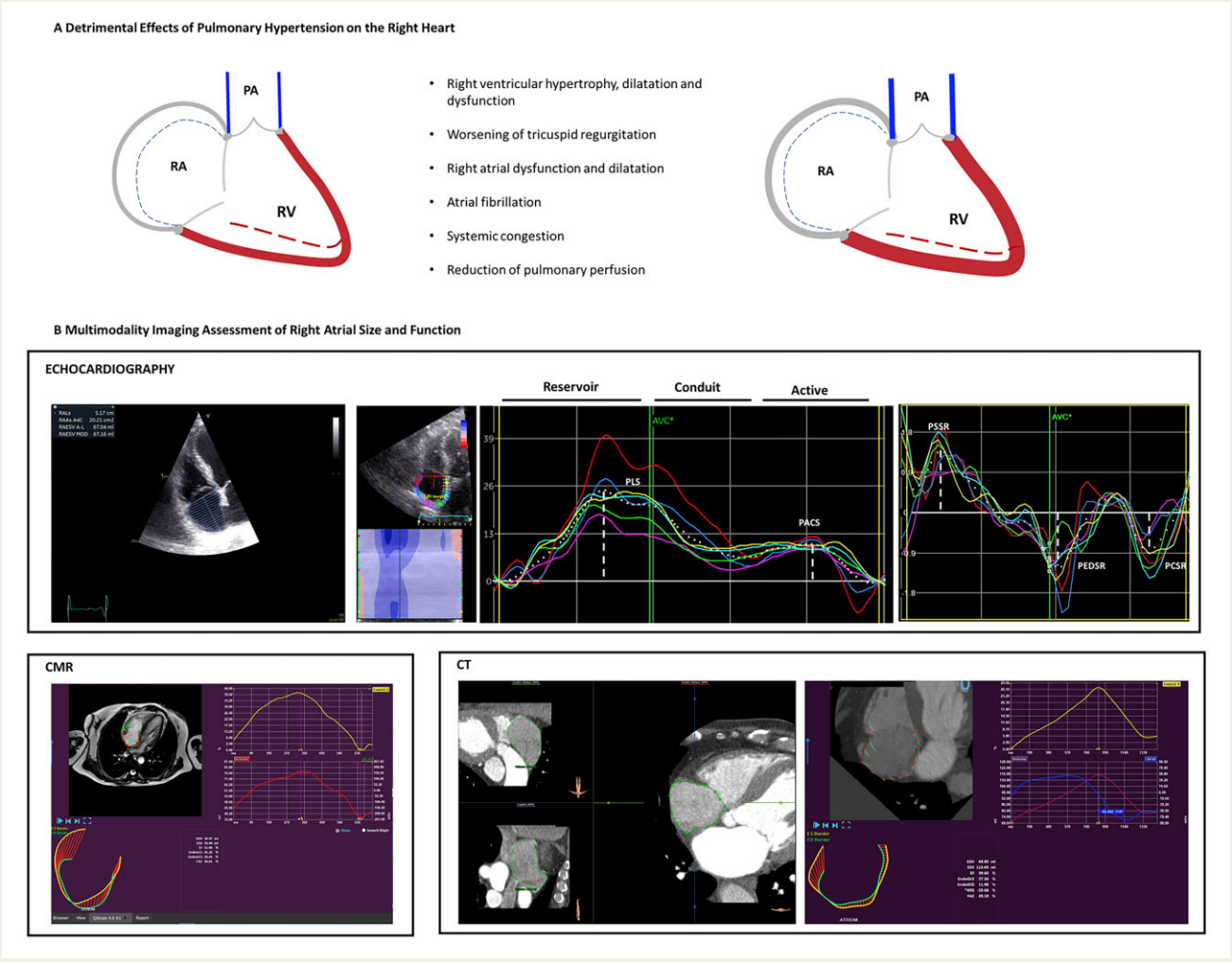

Figure 5 Multi-modality imaging assessment of the RA in pulmonary hypertension. (*A*) The detrimental effects of pulmonary hypertension on the right heart. Red dashed lines represent the RV end-systolic volume, whereas the black dotted lines depict the RA end-diastolic volume Panel B illustrates multimodality imaging assessment of right atrial size and function using bi-dimensional echocardiography, CMR, and CT. RA end-systolic area and volume are assessed from an apical four-chamber view focused on the right heart using echocardiography. The same view is used to assess RA function using speckle tracking echocardiography. The following parameters are usually evaluated to assess RA function, PLS, and PSSR to investigate reservoir function; PACS and PCSR for active atrial contraction; and finally, the difference between PLS and PACS, and PEDSR for the conduit phase. A CMR four-chamber view is used to assess atrial phasic volumes and function based on feature-tacking derived RA strain. Similarly, CT is applied to assess RA size and function. AVC, aortic valve closure; PA, pulmonary artery; RV, right ventricle.

was reported to be 42 ± 9% and 45 ± 10% for men and women, respectively,[5] while another study reported similar values of 44.6 ± 12.5% and 47.0 ± 13.4%, respectively.[20] With 3D echocardiography, total RA EmF has been reported in two studies to be 61 ± 8% and 52.5 ± 6.5% for men and 65 ± 8% and 53.3 ± 6.9% for women.[20]

CMR and CT measurements of RA size and function

The technical strengths and limitations of non-invasive imaging modalities currently used for RA assessment are summarized in *Table 3*. CMR is the accepted gold standard for cardiac chamber volumetric assessment, providing both structural and functional information without associated ionizing radiation, and greater temporal resolution when compared with CCT. Yet, CMR has lower spatial resolution and requires longer acquisition times than CCT. A steady-state free precession is the most used technique in CMR for the acquisition of cine-images of the RA. RA area, longitudinal, and transverse diameters are typically obtained from the four-chamber and the RV two-chamber views, which are routinely acquired during CMR exams. RA volumes can be measured in these views by using the biplane area–length method[38] (*Figure 6*). The modified Simpson's method and 3D-volumetric modelling can be performed by tracing the endocardial border in all contiguous slices on a stack of RA short-axis cine images using a slice thickness between 5 and 8 mm but comes at the expense of prolonged post-processing times. More precise 3D volume estimation by CMR can also be obtained with dedicated software that is capable of auto-detecting endocardial borders.[39] IVC and SVC contours should be excluded from the

Table 2 Summary of the key echocardiography studies of RA size and function

First author, year (reference)	Population, methods	Parameters	Total	Male	Female
Current guidelines					
Lang, 2015[24]	Guidelines	Indexed 2D RA minor axis (mm/m^2)		19 ± 3	19 ± 3
		Indexed 2D RA major axis (mm/m^2)		24 ± 3	25 ± 3
		Indexed 2D ES RAV (mL/m^2)		25 ± 7	21 ± 6
Key studies					
Wang, 1984[28]	– 54 normal volunteers – Age 20–66 years – USA – Single-centre study	2D ES RAV (mL)		39 ± 12	27 ± 7
Aune, 2009 [29]	– 166 healthy subjects – 48% male – Age 29–79 years – 3D TTE – Echocardiography machine: Philips; Software: Philips – Norway (Europe) – Single-centre study	Indexed 2D ES RAV (mL/m^2) Indexed 2D ED RAV (mL/m^2) 3D RA total emptying fraction (%)	18–47 5–20 46–80	18–50 7–22 46–74	17–41 5–18 48–83
D'Oronzio, 2012[30]	– 1625 subjects with normal echocardiography studies – Mean ± SD age 44 ± 14 years – 47% men – 2D TTE – Switzerland (Europe) – Single-centre study	Indexed 2D RA minor axis (mm/m^2) Indexed 2D RA major axis (mm/m^2)		19 ± 3 24 ± 3	19 ± 3 25 ± 3
Padeletti, 2012[15]	– 84 healthy individuals – 30% of patients >40 years – 41% men – Echocardiography machine: General Electric; Software: General Electric – Italy (Europe) – Single-centre study	2D ES RAV (mL) 2D RA reservoir strain (%)	34 ± 11 49 ± 13		
Peluso, 2013[16]	– 200 healthy volunteers – Mean ± SD age 43 ± 15 years – 44% men – 2D TTE, Strain, 3D TTE – Echocardiography machine: General Electric; Software: General Electric – Italy (Europe) – Single-centre study	2D ES RAV area–length method (mL) Indexed 2D ES RAV (area–length) (mL/m^2) 2D Pre-A RAV (area–length) (mL) Indexed 2D Pre-A RAV (area–length) (mL/m^2) 2D ED RAV (area–length) (mL) Indexed 2D ED RAV (area–length) (mL/m^2) 3D ES RAV (mL) Indexed 3D ES RAV (mL/m^2) 3D Pre-A RAV (mL) Indexed 3D Pre-A RAV (mL/m^2) 3D ED RAV (mL) Indexed 3D ED RAV (mL/m^2) 3D RA total emptying fraction (%) 3D RA passive emptying fraction (%) 3D RA active emptying fraction (%) 2D RA reservoir strain (%) 2D RA conduit strain (%) 2D RA contractile strain (%)	41 ± 14 23 ± 7 27 ± 11 15 ± 5 17 ± 7 10 ± 4 52 ± 15 29 ± 7 28 ± 10 16 ± 5 19 ± 8 11 ± 4 63 ± 9 46 ± 11 31 ± 8 44 ± 10 27 ± 9 –17 ± 4	50 ± 15 26 ± 7 33 ± 11 17 ± 5 21 ± 7 11 ± 4 60 ± 16 31 ± 8 34 ± 10 18 ± 5 24 ± 8 12 ± 4 61 ± 8 44 ± 10 29 ± 7 42 ± 9 25 ± 9 –17 ± 4	35 ± 10 21 ± 6 22 ± 8 13 ± 4 14 ± 5 8 ± 3 45 ± 11 27 ± 6 24 ± 7 14 ± 4 16 ± 5 9 ± 3 65 ± 8 48 ± 12 33 ± 9 45 ± 10 28 ± 10 –17 ± 4
Kou, 2014[18]	– 734 normal European subjects – 43% men – Mean ± SD age 45.8 ± 13.3 years – 2D TTE – Echocardiography machine: General Electric, Philips – NORRE study – Europe – Multicentre study	2D RA minor axis (mm) Indexed 2D RA minor axis (mm/m^2) 2D RA major axis (mm) Indexed 2D RA major axis (mm/m^2) 2D ES RA area (cm^2/m^2) Indexed 2D ES RA area (cm^2/m^2) 2D ES RAV (area–length) (mL) Indexed 2D ES RAV (area–length) (mL/m^2) 2D ES RAV (Simpson) (mL) Indexed 2D ES RAV (Simpson) (mL/m^2)	36.1 ± 5.6 20.0 ± 2.9 45.9 ± 5.4 25.5 ± 3.0 14.5 ± 3.2 8.0 ± 1.5 40.1 ± 14.7 21.9 ± 7.1 37.5 ± 13.5 20.6 ± 6.5	38.4 ± 5.4 19.8 ± 2.8 48.1 ± 4.7 24.8 ± 2.5 16.1 ± 2.9 8.3 ± 1.4 46.9 ± 14.5 24.1 ± 7.0 43.8 ± 13.4 22.5 ± 6.5	34.2 ± 5.1 20.2 ± 3.0 44.1 ± 5.3 26.1 ± 3.2 13.2 ± 2.9 7.8 ± 1.6 34.4 ± 12.4 20.2 ± 6.7 32.5 ± 11.4 19.0 ± 6.2
Ruohonen, 2016[19]	– 1079 healthy volunteers – 41% men – Mean age: 40.9 ± 5.1 (men); 41.3 ± 5.0 (women) – 2D TTE – Echocardiography machine: Acuson Sequoia, Software: ComPACS 10.7.8 – Finland (Europe) – Multicentric study	2D RA minor axis (mm) 2D RA major axis (mm) 2D ES RAV (area–length) (mL) Indexed 2D ES RAV (area–length) (mL/m^2)		41.0 ± 52 53.3 ± 5.7 57.7 ± 17.9 28.8 ± 8.6	35.8 ± 4.5 49.3 ± 4.9 40.4 ± 11.9 23.2 ± 6.5
Brand, 2018[23]	– 123 women without known cardiovascular diseases or risk factors – Echocardiography machine: General Electric; Software: General Electric	RA reservoir strain (%) RA conduit function (%) RA contraction strain (%)			44.9 ± 11.6 27.1 ± 9.5 17.0 ± 5.9

Continued

Table 2 *Continued*

First author, year (reference)	Population, methods	Parameters	Total	Male	Female
	– Berlin (Germany)				
	– Cross-sectional randomized trial				
Ferrara, 2018[17]	– 596 healthy subjects	2D RA major axis (mm)	43.0 ± 4.7	45.5 ± 4.6	41.5 ± 4.0
	– mean age 45.7 ± 14.6 years	Indexed 2D RA major axis (mm/m^2)	24.6 ± 2.8	24.9 ± 2.6	24.1 ± 3.1
	– 40% men	2D RA minor axis (mm)	32.1 ± 4.8	35.6 ± 4.2	29.8 ± 3.7
	– 2D TTE	Indexed 2D RA minor axis (mm/m^2)	18.3 ± 2.7	18.8 ± 2.6	17.9 ± 2.7
	– Echocardiography machine: General Electric; Software: General Electric	2D ES RAV (area–length) (mL)	36.8 ± 9.2	43.2 ± 8.6	32.4 ± 7
		Indexed 2D ES RAV (area–length) (mL/m^2)	20.7 ± 4.2	22.7 ± 4.3	19.3 ± 3.7
	– Italy (Europe)	2D ES RAV Simpson (mL)	21.6–51.9	29.0–57.3	20.8–43.9
	– Single-centre study	Indexed 2D ES RAV Simpson (mL/m^2)	13.7–27.6	15.6–29.7	13.2–25.3
Nemes, 2020[31]	– 150 subjects	3D ES RAV (mL)	46.8 ± 14.7		
	– Mean±SD age 31.0 ± 11.6 years	Indexed 3D ES RAV (mL/m^2)	25.5 ± 8.1		
	– 52% male	3D Pre-A RAV (mL)	33.3 ± 11.3		
	– RA volumetric data derived from 3D speckle-tracking echocardiography	Indexed 3D Pre-A RAV (mL/m^2)	18.1 ± 5.8		
		3D ED RAV (mL)	26.0 ± 10.0		
		Indexed 3D ED RAV (mL/m^2)	14.1 ± 5.0		
	– Echocardiography machine: Toshiba				
	– Software: Toshiba				
	– Hungary (Europe)				
	– Single-centre study				
Soulat-Dufour, 2020[20]	– 2008 healthy adults	RA ES longitudinal dimension (mm)	43.4 ± 5.0	44.7 ± 5.1	42.0 ± 4.4
	– 18–40 years (n = 854), 41–65 years (n = 653), and >65 years (n = 501)	Indexed RA ES longitudinal dimension (mm/m^2)	24.6 ± 2.9	23.8 ± 2.6	25.5 ± 2.9
		RA ES transverse dimension (mm)	35.0 ± 5.3	36.7 ± 5.4	33.2 ± 4.6
	– 2D TTE, Strain, 3D TTE	Indexed RA ES transverse dimension (mm/m^2)	19.8 ± 2.8	19.5 ± 2.8	20.1 ± 2.7
	– Echocardiography machine: Philips, General Electric, Siemens	2D ES RAV (mL)	34.6 ± 12.7	39.1 ± 13.6	29.8 ± 9.6
		Indexed 2D ES RAV (mL/m^2)	19.4 ± 6.0	20.6 ± 6.4	18.0 ± 5.3
	– Software: Tomtec (Philips)	3D ES RAV (mL)	39.2 ± 14.8	43.9 ± 15.7	34.0 ± 11.7
	– WASE Normal Values Study International (34.9% white, 41.6% Asian, 9.7% black)	Indexed 3D ES RAV (mL/m^2)	21.9 ± 7.1	23.2 ± 7.4	20.5 ± 6.4
		3D Pre-A RAV (mL)	26.2 ± 11.0	29.6 ± 11.7	22.5 ± 8.9
		Indexed 3D Pre-A RAV (mL/m^2)	14.7 ± 5.5	15.6 ± 5.7	13.6 ± 5.0
	– Multicentre study	3D ED RAV (mL)	18.4 ± 7.4	20.8 ± 7.8	15.8 ± 5.9
		Indexed 3D ED RAV (mL/m^2)	10.3 ± 3.6	11.0 ± 3.8	9.6 ± 3.3
		3D total emptying RAV (mL)	16.9 ± 11.0	19.2 ± 11.9	14.6 ± 9.4
		3D passive emptying RAV (mL)	10.6 ± 8.3	11.9 ± 9.1	9.2 ± 7.3
		3D active emptying RAV (mL)	6.3 ± 4.8	7.3 ± 5.2	5.3 ± 4.0
		3D total emptying fraction (%)	52.9 ± 6.7	52.5 ± 6.5	53.3 ± 6.9
		3D passive emptying fraction (%)	32.8 ± 12.9	32.2 ± 12.4	33.5 ± 13.3
		3D active emptying fraction (%)	29.0 ± 5.9	29.2 ± 5.7	28.9 ± 6.1
		RA reservoir strain (%)	45.8 ± 13.0	44.6 ± 12.5	47.0 ± 13.4
		RA conduit strain (%)	–18.4 ± 7.5	–17.8 ± 7.0	–19.1 ± 7.9
		RA contractile strain (%)	–27.6 ± 9.7	–27.0 ± 9.3	–28.2 ± 10.1

Values are expressed as mean ± SD or normal reference ranges (95% confidence intervals).
ED, end-diastolic; ES, end-systolic; NORRE, NOrmal Reference Ranges for Echocardiography; Pre-A, before atrial contraction; RA, right atrium/atrial; RAV, right atrial volume; SD, standard deviation; TTE, transthoracic echocardiography; WASE, World Alliance Societies of Echocardiography.

tracing, as well as the appendage.[38–41] Normal ranges for RA size vary significantly between methods. The area–length method is faster, but less reproducible compared to other volumetric methods. Volumetric methods are more accurate and provide larger values than the area–length method.

Intra-observer variability has been reported at 3.5% for RA volumes, 3.6% and 1.8% for areas in the two- and four-chamber views, and ∼4% for longitudinal and transverse diameters in the four- and two-chamber views, respectively. Inter-observer variability has been reported to be 3.9% for RA volumes, 5.2% and 5% for areas in the two- and four-chamber views, respectively, and 5.5% for longitudinal and transverse diameters in the four- and two-chamber views, respectively. RA reference values indexed to BSA are similar between men and women. There is a minimal decrease in RA size with age in healthy subjects, with some studies indicating that ethnicity should be interpreted in context as well.[39,40] There is moderate correlation and wide limits of agreement between MRI and CCT, ranging from ±13 to ±29 mL for RA volumes.[42] Normal reference values for RA size by CMR are listed in *Table 4*. Age-related changes in blood flow and geometry of the caval veins and RA have been recently described using 4D flow CMR. These age-related changes have a significant impact on the haemodynamics of the RA inflow tract. In young subjects, blood flow of the RA showed a clockwise rotating helix without signs of turbulence. In contrast, this rotation was absent, and turbulences were more frequent in older subjects.[43]

Reference values of RA size obtained using CCT are limited and not universal. End-systolic RA volume using 64-slice CCT in 103 healthy subjects were found to be 111.9 ± 29 mL with a reference range of 54.9–168.9 mL by Lin *et al.*[44] In the study by Takahashi *et al.*[45] with 320-slice CCT and semi-automated 3D segmentation technique, maximum RA volume was 82.1 ± 44.1 mL. Standard four-chamber and right ventricular two-chamber views are used for linear measurements. Linear measurements and volume calculations are performed in a similar way to CMR, including longitudinal, transverse and sagittal diameters, direct volume measurements (Simpson's method), area–length method, and ellipsoid method for volume quantification.[46] Artefacts due to peculiarities of contrast use and

Table 3 Strengths and limitations of TTE, CMR, and CCT in the assessment of right atrium

	TTE	CMR	CCT
Logistic characteristics			
Accessibility	+++	+	+++
Portability	+++		
Technical characteristics			
Spatial resolution	+	++	+++
Temporal resolution	+++	++	+
Contrast material			Required
Strengths			
	– Real-time anatomical and functional evaluation	– Structural and functional information in a single study	– Short scan time in a single breath-hold
Limitations			
	– Operator dependent – Limited acoustic windows often related to body habitus	– Claustrophobia – Contraindications to MR – Long scan time	– Contraindicated in pregnancy – Limited hemodynamic evaluation – Exposure to ionizing radiations

CMR, cardiac magnetic resonance; CCT, cardiac computed tomography; TTE, transthoracic echocardiography.

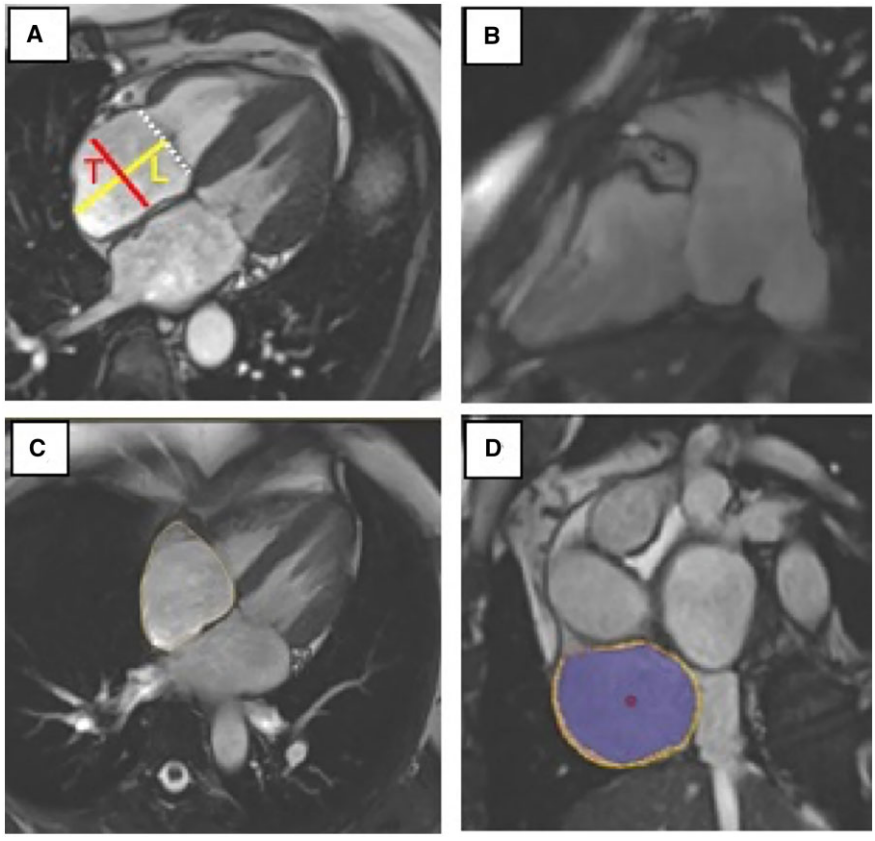

Figure 6 RA quantification by CMR. (*A*) four-chamber, (*B*) two-chamber views with longitudinal diameter (L) between tricuspid annular plane and the roof of RA transverse diameter (T) bisects L perpendicularly. (*C*) RA endocardial tracing in four-chamber view including right atrial appendage for RA area calculation. (*D*) RA blood pool can be traced in the stack of atrial SAX images at atrial diastole and systole for calculation of right atrial volumes and EmF. Courtesy of Dr Cemil İzgi.

Table 4 Normal reference values for right atrial size by CMR

		Men		Women	
		Mean ± SD	Range	Mean ± SD	Range
Max area (cm^2/m^2, two-chamber)		12 ± 2	7–17	12 ± 2	7–17
Max area (cm^2/m^2, four-chamber)		11 ± 2	7–15	12 ± 2	8–15
Max long diameter (cm/m^2, two-chamber)		3 ± 0.4	2.3–3.7	3.2 ± 0.4	2.3–4.1
Max transverse diameter (cm/m^2, two-chamber)		2.3 ± 0.5	1.3–3.3	2.6 ± 0.6	1.5–3.7
Max long diameter (cm/m^2, four-chamber)		2.9 ± 0.4	2.2–3.7	3.2 ± 0.4	2.4–4.0
Max transverse diameter (cm/m^2, four-chamber)		2.6 ± 0.3	2.1–3.2	2.7 ± 0.3	2.0–3.4
Biplane area–length method (excluding appendage)	Max volume (mL/m^2)	38 ± 12	15–61	35 ± 10	16-54
	Min volume (mL/m^2)	19 ± 7	5–32	15 ± 5	6–24
Simpson's method (excluding appendage)	Max volume (mL/m^2)	52 ± 12	28–76	51 ± 10	31–71
	Min volume (mL/m^2)	27 ± 9	9–45	23 ± 6	12–35
	Ejection fraction (%)	49 ± 10	29–69	54 ± 9	36–72
3D modelling (excluding appendage)	Max volume (mL/m^2)	55 ± 10	33–78	53 ± 10	36–70

From Kawel-Boehm *et al.*[42] and Maceira *et al.*[39]
Long, longitudinal; Max, maximum; Min, minimum.

excess cardiac motion may lead to errors in volume calculations. Therefore, tailored injection protocols are advised for an adequate visualization of the right atrium (RA). On the other hand, the excellent spatial resolution of CCT enables detailed anatomic evaluation of the RA, especially when performed with electrocardiographic gating (*Figure 7*). Disadvantages of CCT include exposure to ionizing radiation and iodinated contrast agents. CCT contrast protocols are mostly limited to diastole, while optimal assessment of RA size, remodelling, and systolic function requires full-cycle retrospectively gated acquisition. Arrhythmias can compromise the accuracy and reproducibility of the quantification and increase radiation exposure. It is also important to emphasize that currently, there is no clear consensus regarding which of the imaging modalities is superior in the assessment of RA dimensions.

The RA in atrial fibrillation

In the realm of atrial fibrillation (AF), most of the echocardiographic literature has focused on the phenomenon of left atrial remodelling[47–50] and incident stroke prediction.[51–54] This may be somewhat monolithic, as it is evidence that AF involves both atria, but the associated pathophysiology of the RA in AF has yet to be thoroughly investigated. The purpose of this section is to describe the different purported mechanisms regarding the role of RA in the pathogenesis of AF.

AF and RA remodelling

Atrial remodelling in AF is a complex phenomenon. Structural, electrical, and metabolic RA remodelling have all been described as responsible for the link between RA and AF. In a population free of clinical cardiovascular disease, CMR-derived RA volumes were independently associated with incident AF, even after adjusting for conventional cardiovascular risk factors and left atrial parameters.[55] Interestingly, following the restoration of sinus rhythm in AF, anatomical, and/or functional reverse remodelling has been noted in both the left and right atria.[56–59] In a population of endurance male athletes, the presence of higher RA volumes, and lower reservoir strain were associated with increased risk of paroxysmal AF.[60] In animal models of AF where remodelling was initiated by endurance exercise[61] and/or pulmonary hypertension (PH)[62] both left atrial and RA fibrosis were present and associated with increased AF susceptibility. Interestingly, investigators have described a subtype of AF originating from the RA,[63] which appears to be accompanied by specific RA structural remodelling patterns including a large RA appendage, less remodelled left atrium, and lower burden of epicardial adipose tissue surrounding the atria.[64]

Besides RA structural remodelling, RA electrical remodelling has also been described. In a murine model of PH with AF, studies demonstrated that RA conduction slowing was coupled with greater AF inducibility when compared with controls.[62] Additional studies described paroxysmal AF initiated by RA ectopy and maintained by a re-entrant circuit localized in the RA (so-called RA fibrillation).[63] In patients with chronic obstructive pulmonary disease (COPD) and concurrent AF, electrophysiological studies demonstrated that the slowing of RA conduction and a higher prevalence of non-pulmonary vein foci were localized in the RA.[65–67] In patients with persistent AF and left ventricular (LV) systolic dysfunction who underwent successful catheter ablation, long-term RA electrical remodelling analysis showed a recovery in the electrical atrial changes.[58]

Molecular analyses in AF have shown the expression of specific metabolic markers in the RA. In rats with PH and AF, activation of hypertrophic, proinflammatory, and profibrotic pathways were noted in the RA, akin to animal models of RA remodelling caused by LV dysfunction due to myocardial infarction.[62] In a different study using the same rat model of PH and AF, the inflammation-resolution promoting molecule (RvD1) showed suppression of AF promotion, and attenuation of atrial fibrosis.[68] Other studies have shown that sustained adenosine-induced AF was driven by localized re-entry circuits in

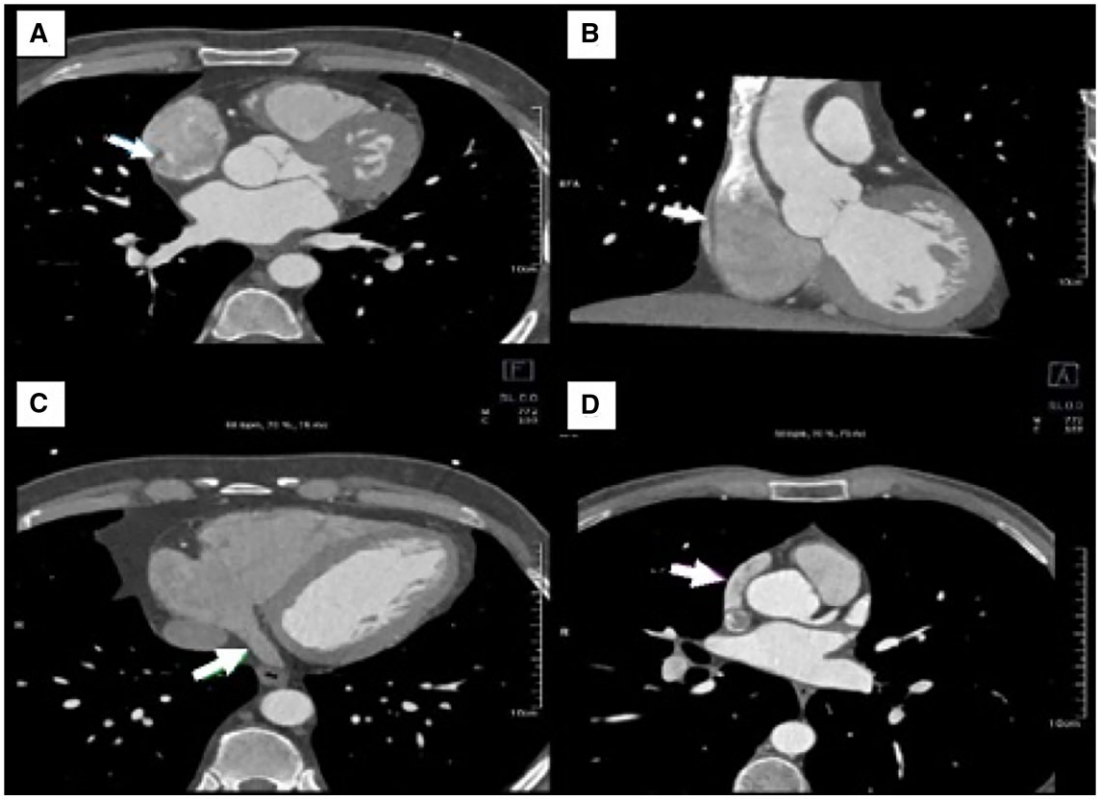

Figure 7 Axial and coronal ECG-gated cardiac CT images demonstrate crista terminalis (*A, B*), coronary sinus (*C*), and RA appendage (*D*). Courtesy of Dr Ibrahim Altin.

areas of the RA with the highest expression of adenosine A1 receptors.[69] Of note, some metabolic general disorders described in patients with AF were derived from analysis primarily focused upon the RA or RA appendage.[70–73]

Recently, Hiram *et al.*,[74] used a monocrotaline-treated rat model demonstrating that the induced right heart disease produces a substrate for AF maintenance due to RA re-entrant activity, with an underlying substrate prominently involving RA fibrosis and conduction abnormalities. The authors emphasize some of the interesting differences compared with the AF substrate in LV dysfunction post-myocardial infarction. These differences provide new mechanistic insights and point to new approaches and tools for therapeutic interventions.[62]

Aetiologies of RA remodelling leading to AF

As described in the pathophysiology of the RV,[75] RA remodelling occurs across a spectrum of clinical settings (i.e. pressure overload, volume overload, and intrinsic cardiomyopathy) leading to an underlying arrhythmogenic substrate and AF.

The pressure overloaded RA and AF

Several pulmonary diseases can induce RA pressure overload which may lead to RA structural, electrical, or metabolic remodelling, and subsequent AF[76] (*Figure 8*).

Atrial arrhythmias are frequently encountered in PH and appear to connote a worse clinical outcome. In clinical studies, the prevalence of AF in PH was estimated to be as high as 31%.[77] Moreover, elevated RA pressure and enlarged RA size have been described as established risk factors for adverse outcomes or death in PH.[78,79] In patients with PH and AF, New York Heart Association (NYHA)/World Health Organization (WHO) functional class, 6-min walking distance, NT-pro-B-type natriuretic peptide concentration, and renal function were significantly compromised compared to patients with PH and sinus rhythm.[77] Persistent AF has been associated with the risk of death from RV failure in PH patients.[80]

COPD is another disease state well-associated with an increased risk of AF. In a large, retrospective cohort of patients on home oxygen admitted for COPD exacerbation, the prevalence of AF was 18.2% and served as a risk predictor for in-hospital death.[81] In a multicentre cohort study, COPD was associated with AF and death.[82] Reductions in forced expiratory volume in 1 s and obstructive respiratory disease were associated with higher incidence of AF after adjustment for measured confounders.[83] Of note, patients with AF and concomitant COPD have a more severely impaired RA function compared to AF patients without COPD.[84]

Additional diseases that induce right heart disease are correlated with AF including obstructive sleep apnoea with conduction abnormalities related to connexin dysregulation and fibrosis[85,86]; asthma and lack of asthma control.[87] Finally, recent data also underscored

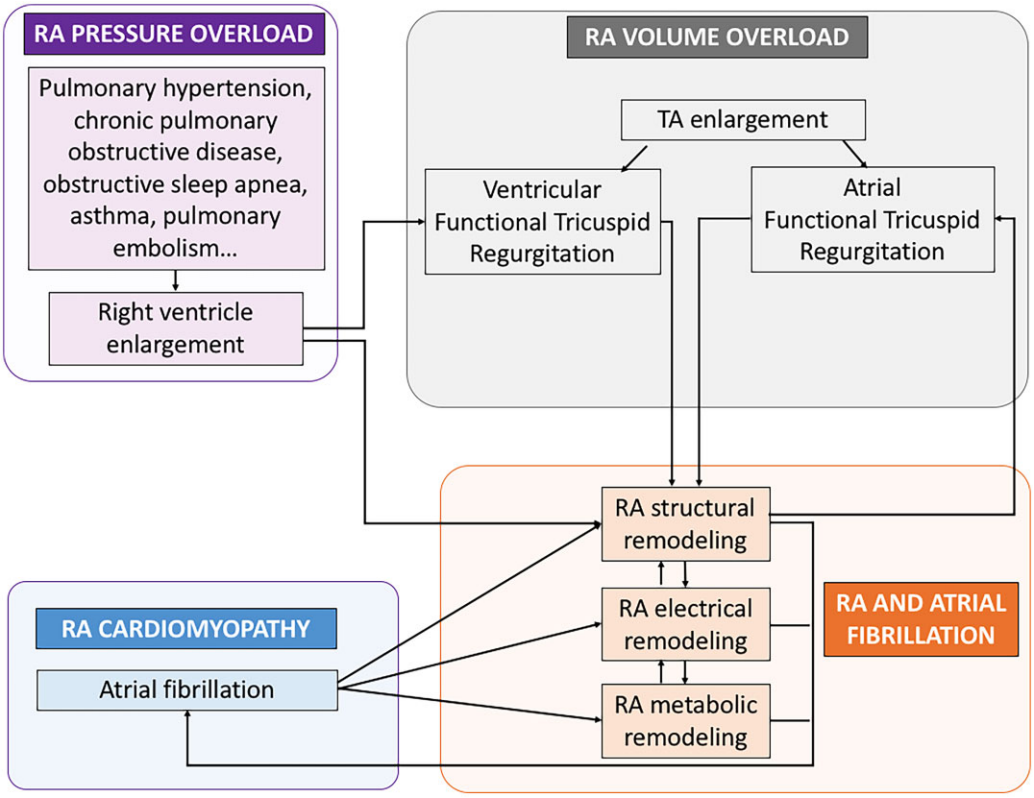

Figure 8 Proposed mechanism linking RA and AF.

the link between AF and the risk of pulmonary embolism and deep vein thrombosis during the first months after AF diagnosis.[88] Gaynor *et al*., used a dog model of RA and RV pressure and volume overload and recorded findings after 3 months of progressive pulmonary artery banding. The authors demonstrated that RV systolic pressure was usually preserved, but diastolic function became impaired. To compensate, RA contractility increased, and the RA become more distensible to maintain filling of the stiffened ventricle. This compensatory response to the RA likely plays an important role in preventing clinical failure in chronic PH.[89]

The volume-overloaded RA and AF

The presence of functional tricuspid regurgitation (FTR) is a key element in RA volume overload states resulting in RA structural, electrical, or metabolic remodelling, which may lead to AF (*Figure 8*).

Patients in AF without severe FTR have been described as having RA and tricuspid annulus remodelling, independent of the presence of left heart disease.[90] Accordingly, it has been hypothesized that FTR could be either considered as the cause or consequence of RA dilatation and AF development.[91] In patients in AF with FTR, a significant correlation has been demonstrated between FTR severity and RA volume and tricuspid annulus area.[92] Irrespective of cardiac rhythm and RV loading conditions, RA volume is a major determinant of tricuspid annulus area in patients with FTR, and RA enlargement is an important mechanism for tricuspid annulus dilatation.[93]

Two distinct mechanisms should be noted for FTR in AF: (i) in ventricular FTR, a combination of remodelling and dysfunction of the RV, dilatation of the tricuspid annulus, and tethering of the tricuspid valve leaflets; and (ii) atrial FTR in patients with normal RV geometry and function but with dilated tricuspid annulus and RA (*Figure 8*).

Ventricular functional tricuspid regurgitation

Ventricular FTR may induce RA remodelling leading to AF (*Table 5*). In a healthy population, morphologic analysis of the normal RV using 3D echocardiography-derived curvature indices has been reported in strategies to describe differing RV morphologies with distinct implications in heart failure, PH, and left-to-right interatrial shunt.[94] In PH, RV elongation, and elliptical/spherical RV deformation induced valvular tethering leads to ventricular FTR (*Figure 9*).[96] Other studies have reported the role of tricuspid annulus dilatation and/or papillary muscles displacement in the development of ventricular FTR,[96] as well as an observation of a more circular tricuspid annulus shape in comparison with healthy subjects.[97]

Atrial functional tricuspid regurgitation

Though more recently described, atrial FTR (*Table 5*) is probably the cornerstone of RA remodelling in AF (*Figure 9*). In cases of atrial FTR, 3D echocardiography has demonstrated a larger tricuspid annular area, weaker annular contraction, smaller tethering angle, and similar leaflet coaptation status when compared with patients with FTR and left-sided heart disease.[98] Interestingly, tricuspid annular area in mid-

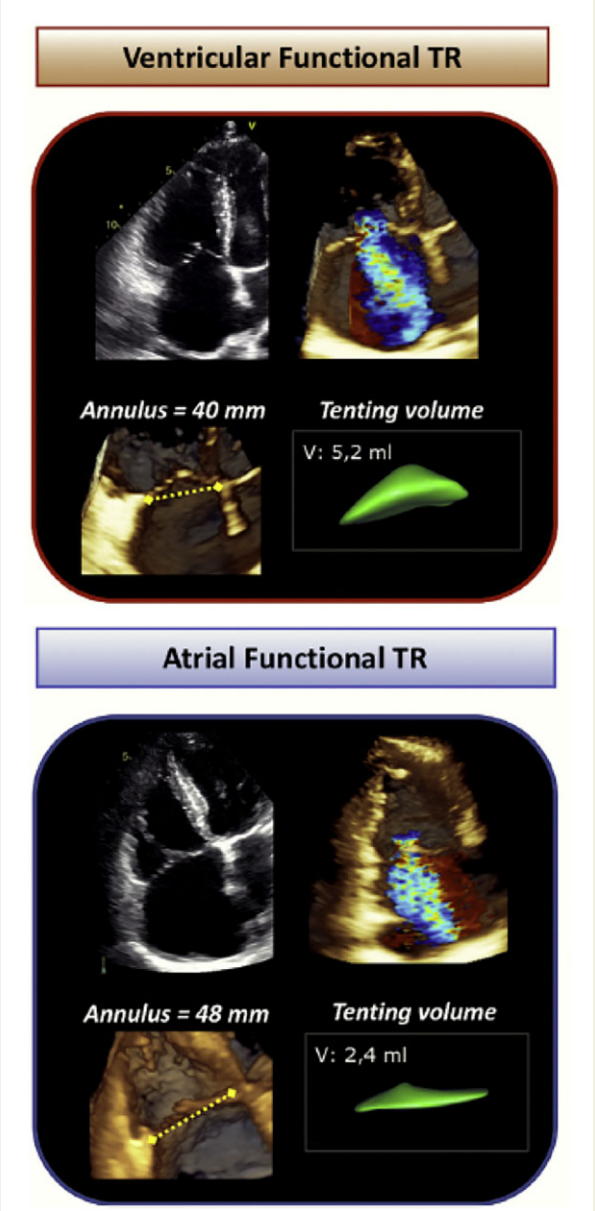

Figure 9 Ventricular FTR in patients with pulmonary arterial hypertension (left) and atrial FTR (right) with AF that resulted in RA remodelling leading to AF. Modified from Ref.[56] Adapted from Muraru *et al.*[95] AF, atrial fibrillation; FTR, functional tricuspid regurgitation; RA, right atrium; TR, tricuspid regurgitation.

systole was independently associated with atrial FTR and the tricuspid annulus area in atrial FTR was more closely correlated with the RA volume than the RV volume.[98] Thus, in contrast to ventricular FTR, dilatation of the tricuspid annulus appears to be the primary cause of regurgitation in atrial FTR.[99]

The cardiomyopathic RA and AF

AF is the primary example of autonomous disease affecting both atria and is responsible for the development of left and RA cardiomyopathy. Few data are available on the existence of an intrinsic RA cardiomyopathy in conjunction with other cardiovascular diseases. This compelling but preliminary hypothesis should be evaluated further investigations in different clinical settings (e.g. myocardial infarction, arrhythmogenic RV cardiomyopathy, amyloidosis, myocarditis, cardiotoxicity) due to different conditions, such as chemotherapy. RA remodelling in heart failure with preserved ejection fraction is associated with higher prevalence of AF, mild tricuspid regurgitation, severe PH, and impaired reservoir function.[100]

The RA in PH

In the early phase of PH, the increased RV afterload induces RV remodelling which is mainly characterized by hypertrophy. As PH progresses, RV dysfunction and dilatation, which represent the main maladaptive features of this disease, may begin and eventually lead to RV failure.[101] RV overload and increased RV stiffness then leads to a proportional increase in RA pressure. In addition, RV dilatation can cause FTR through annular dilatation and leaflet tethering, which in turn may further increase RA pressure.[99] As such, increased RA pressure determines RA remodelling, dysfunction, dilatation, and eventually failure with worsening of RV filling, pulmonary perfusion, and systemic congestion (*Figure 5A*).

Non-invasive cardiac imaging and prognostic role of right atrial size and function

Current guidelines recommend the evaluation of RA size and pericardial effusion as the only imaging markers for risk stratification in PH.[102] A dilated RA has been associated with poor prognosis in patients with PH.[103] Indeed, in a small cohort of 25 consecutive patients with PAH, RA area, and presence of FTR were independently related to mortality or eventual lung transplantation during a mean follow-up of 29 months.[104] Furthermore, in a cohort of 66 consecutive PH patients, RA volume was positively associated with RV afterload assessed by echocardiography (i.e. pulmonary artery systolic pressure).[105] Therefore, RA area quantified on a four-chamber view with either echocardiography or CMR, is suggested in the current guidelines as one of the criteria for risk stratification in patients with PH. The proposed cut-off values of 18 and 26 cm^2 for RA area should be used to identify patients with PH at intermediate- (5–10%) or high risk (> 10%) of 1-year mortality, respectively. It is prudent to emphasize that these recommendations are based on relatively small studies. In addition, the proposed cut-off values are predominantly derived from expert consensus opinion, and they differ notably from the cardiac chamber quantification guidelines which recommend an indexed RA volume with the following sex-specific cut-off values for RA dilatation of 39 and 33 mL/m^2 for males and females, respectively.[24] The PH guidelines also suggest assessment of RA area for follow-up risk stratification, evaluation of the effect of specific therapies and to eventually intensify PH-specific treatments. More advanced measures of RA size with 3D echocardiography, such as the 3D RA minimum volume combined with the 3D assessment of the left atrial size, showed to be useful to distinguish between pre-capillary and post-capillary PH,[106] therefore, having potential implications on choice of PH treatment.[102]

Table 5 Differences between ventricular functional and atrial functional TR

Parameter	VFTR	AFTR
Leaflet tethering	+++	+
TA size	+	+++
RA volume	Variable dilatation	+++
RV basal diameter	+++	+
RV mid diameter	+++	Normal or mild dilatated
RV length	Enlarged	Normal or decreased
RV shape	Elliptical	Conical
RV function	Frequently decreased	Minimally decreased or normal
Pulmonary hypertension	Present or absent	Absent
Left heart disease	Present or absent	Absent

AFTR, atrial functional tricuspid regurgitation; RA, right atrial; RV, right ventricular; TA, tricuspid annulus; VFTR, ventricular functional tricuspid regurgitation.

In addition to size, RA function appears to play a pivotal role in the prediction of the symptom development as well as prognosis in patients with PH.[107] In 65 patients with PH from the IMPRES (Imatinib in Pulmonary Arterial Hypertension) trial, RA reservoir and conduit function assessed with longitudinal strain were impaired in patients with PH compared to healthy controls. In the same study, RA reservoir function was associated with RV enlargement and dysfunction as well as N-terminal pro-brain natriuretic peptide (NT-proBNP), independently of RA size and pressure.[108] This suggests an incremental value of RA function over RA size parameters in assessing decompensation in PAH.[108] Regarding prognostic value, prior work demonstrated an association of all RA speckle tracking echocardiography strain-derived phasic functions with hospitalizations or death during a median follow-up of 44 months in a prospective cohort of 63 consecutive patients with PAH.[109] Similarly, in a cohort of 80 PAH patients, there was an association observed between CMR feature tracking-derived RA function parameters and haemodynamic status, with RA conduit function demonstrating the highest predictive value for adverse events.[110] Furthermore, a recent study showed an increase of RA reservoir and conduit function assessed with CMR after balloon pulmonary angioplasty in a cohort of 29 patients with chronic thromboembolic PH, representing RA functional recovery. These findings correlated well with a decrease in pulmonary vasculature resistance and NT-proBNP levels and was associated with a significant improvement in functional capacity, thus confirming the role of RA in the pathophysiology of PH-related symptoms.[111]

RA peak longitudinal strain has additive prognostic usefulness to other clinical measures, including RV strain, RA area, and RA pressure, in patients with PH. RA mechanical function by strain imaging has the potential for clinical applications in adult and paediatric patients with PH.[112–114]

Future perspectives

The importance of RA size and function has so far been predominantly investigated in patients with pre-capillary PH using echocardiography. Evaluation of the RA in different patient cohorts, such as patients with combined pre- and post-capillary PH or the evaluation of PH-specific treatments on RA morphology and function using additional imaging modalities, such as CT represent important areas for future investigations.

Clinical implications of a comprehensive assessment of the RA

The RA is the cardiac chamber that has been least well studied, even though recent data have shown that changes in RA structure and function have prognostic implications in specific cardiac diseases such as heart failure and PH. In addition, the recently published normative on RA size and function will likely shed light on the role of RA volume in tricuspid annular dilation, AF, and FTR.

Conflict of interest: Three of the authors are on speakers' bureaus of three different companies: RML and FFF for Philips Healthcare, and LES for General Electric. In addition, M.C. has served as a consultant for Novo Nordisk and Astra Zeneca.

References

1. Kucybała I, Ciuk K, Klimek-Piotrowska W. Clinical anatomy of human heart atria and interatrial septum - anatomical basis for interventional cardiologists and electrocardiologists. Part 1: right atrium and interatrial septum. *Kardiol Pol* 2018; **76**:499–509.
2. Sánchez-Quintana D, Anderson RH, Cabrera JA, Climent V, Martin R, Farré J *et al.* The terminal crest: morphological features relevant to electrophysiology. *Heart* 2002;**88**:406–11.
3. Lang RM, Badano LP, Tsang W, Adams DH, Agricola E, Buck T *et al.*; European Association of Echocardiography. EAE/ASE recommendations for image acquisition and display using three-dimensional echocardiography. *J Am Soc Echocardiogr* 2012;**25**:3–46.
4. Faletra FF, Ho SY, Auricchio A. Anatomy of right atrial structures by real-time 3D transesophageal echocardiography. *JACC Cardiovasc Imaging* 2010;**3**:966–75.
5. Matsuyama TA, Inoue S, Kobayashi Y, Sakai T, Saito T, Katagiri T *et al.* Anatomical diversity and age-related histological changes in the human right atrial posterolateral wall. *Europace* 2004;**6**:307–15.
6. Klimek-Piotrowska W, Hołda MK, Koziej M, Hołda J, Piątek K, Tyrak K *et al.* Clinical anatomy of the cavotricuspid isthmus and terminal crest. *PLoS One* 2016;**11**:e0163383.
7. Siddiqui AU, Daimi SR, Gandhi KR, Siddiqui AT, Trivedi S, Sinha MB *et al.* Crista terminalis, musculi pectinati, and taenia sagittalis: anatomical observations and applied significance. *ISRN Anat* 2013;**2013**:803853.
8. Klimek-Piotrowska W, Hołda MK, Koziej M, Strona M. Anatomical barriers in the right atrium to the coronary sinus cannulation. *PeerJ* 2016;**3**:e1548.
9. Teo EY, Ittleman F, Hamlin MP. A Chiari network and difficult cannulation of the coronary sinus for retrograde perfusion. *Anesth Analg* 2010;**111**:79–81.

10. Chang S-L, Tai C-T, Lin Y-J, Ong MG, Wongcharoen W, LO L-W *et al.* The electroanatomic characteristics of the cavotricuspid isthmus: implications for the catheter ablation of atrial flutter. *J Cardiovasc Electrophysiol* 2007;**18**:18–22.
11. Mlynarski R, Mlynarska A, Tendera M, Sosnowski M. Coronary sinus ostium: the key structure in the heart's anatomy from the electrophysiologist's point of view. *Heart Vessels* 2011;**26**:449–56.
12. Holda MK, Klimek-Piotrowska W, Koziej M, Mazur M. Anatomical variations of the coronary sinus valve (Thebesian valve): implications for electrocardiological procedures. *Europace* 2015;**17**:921–7.
13. Cabrera JA, Sanchez-Quintana D, Farre J, Rubio JM, Ho SY. The inferior right atrial isthmus: further architectural insights for current and coming ablation technologies. *J Cardiovasc Electrophysiol* 2005;**16**:402–8.
14. Sanchez-Quintana D, Pizarro G, Lopez-Minguez JR, Ho SY, Cabrera JA. Standardized review of atrial anatomy for cardiac electrophysiologists. *J Cardiovasc Transl Res* 2013;**6**:124–44.
15. Padeletti M, Cameli M, Lisi M, Malandrino A, Zaca V, Mondillo S. Reference values of right atrial longitudinal strain imaging by two-dimensional speckle tracking. *Echocardiography* 2012;**29**:147–52.
16. Peluso D, Badano LP, Muraru D, Dal Bianco L, Cucchini U, Kocabay G *et al.* Right atrial size and function assessed with three-dimensional and speckle-tracking echocardiography in 200 healthy volunteers. *Eur Heart J Cardiovasc Imaging* 2013;**14**:1106–14.
17. Ferrara F, Gargani L, Ruohonen S, Vriz O, Scalese M, Russo V *et al.* Reference values and correlates of right atrial volume in healthy adults by two-dimensional echocardiography. *Echocardiography* 2018;**35**:1097–107.
18. Kou S, Caballero L, Dulgheru R, Voilliot D, De Sousa C, Kacharava G *et al.* Echocardiographic reference ranges for normal cardiac chamber size: results from the NORRE study. *Eur Heart J Cardiovasc Imaging* 2014;**15**:680–90.
19. Ruohonen S, Koskenvuo JW, Wendelin-Saarenhovi M, Savontaus M, Kahonen M, Laitinen T *et al.* Reference values for echocardiography in middle-aged population: the cardiovascular risk in Young Finns Study. *Echocardiography* 2016;**33**:193–206.
20. Soulat-Dufour L, Addetia K, Miyoshi T, Citro R, Daimon M, Fajardo PG *et al.*; WASE Investigators. Normal values of right atrial size and function according to age, sex, and ethnicity: results of the world alliance societies of echocardiography study. *J Am Soc Echocardiogr* 2021;**34**:286–300.
21. Thomas JD, Badano LP. EACVI-ASE-industry initiative to standardize deformation imaging: a brief update from the co-chairs. *Eur Heart J Cardiovasc Imaging* 2013;**14**:1039–40.
22. Cantinotti M, Koestenberger M, Santoro G, Assanta N, Franchi E, Paterni M *et al.* Normal basic 2D echocardiographic values to screen and follow up the athlete's heart from juniors to adults: what is known and what is missing. A critical review. *Eur J Prev Cardiol* 2020;**27**:1294–306.
23. Brand A, Bathe M, Hubscher A, Baldenhofer G, Hattasch R, Seeland U *et al.* Normative reference data, determinants, and clinical implications of right atrial reservoir function in women assessed by 2D speckle-tracking echocardiography. *Echocardiography* 2018;**35**:1542–9.
24. Lang RM, Badano LP, Mor-Avi V, Afilalo J, Armstrong A, Ernande L *et al.* Recommendations for cardiac chamber quantification by echocardiography in adults: an update from the American Society of Echocardiography and the European Association of Cardiovascular Imaging. *J Am Soc Echocardiogr* 2015;**28**:1–39.e14.
25. Asch FM, Banchs J, Price R, Rigolin V, Thomas JD, Weissman NJ *et al.* Need for a global definition of normative echo values-rationale and design of the World Alliance of Societies of Echocardiography Normal Values Study (WASE). *J Am Soc Echocardiogr* 2019;**32**:157–62.e2.
26. Cosyns B, Lancellotti P. Normal reference values for echocardiography: a call for comparison between ethnicities. *Eur Heart J Cardiovasc Imaging* 2016;**17**:523–4.
27. Lancellotti P. Normal reference ranges for echocardiography: do we really need more? *Eur Heart J Cardiovasc Imaging* 2014;**15**:253–4.
28. Wang Y, Gutman JM, Heilbron D, Wahr D, Schiller NB. Atrial volume in a normal adult population by two-dimensional echocardiography. *Chest* 1984;**86**:595–601.
29. Aune E, Baekkevar M, Roislien J, Rodevand O, Otterstad JE. Normal reference ranges for left and right atrial volume indexes and ejection fractions obtained with real-time three-dimensional echocardiography. *Eur J Echocardiogr* 2009;**10**:738–44.
30. D'Oronzio U, Senn O, Biaggi P, Gruner C, Jenni R, Tanner FC *et al.* Right heart assessment by echocardiography: gender and body size matters. *J Am Soc Echocardiogr* 2012;**25**:1251–8.
31. Nemes A, Kormanyos A, Domsik P, Kalapos A, Ambrus N, Lengyel C. Normal reference values of three-dimensional speckle-tracking echocardiography-derived right atrial volumes and volume-based functional properties in healthy adults (Insights from the MAGYAR-Healthy Study). *J Clin Ultrasound* 2020;**48**:263–8.
32. DePace NL, Ren JF, Kotler MN, Mintz GS, Kimbiris D, Kalman P. Two-dimensional echocardiographic determination of right atrial emptying volume: a noninvasive index in quantifying the degree of tricuspid regurgitation. *Am J Cardiol* 1983;**52**:525–9.
33. Kaplan JD, Evans GT Jr, Foster E, Lim D, Schiller NB. Evaluation of electrocardiographic criteria for right atrial enlargement by quantitative two-dimensional echocardiography. *J Am Coll Cardiol* 1994;**23**:747–52.
34. Whitlock M, Garg A, Gelow J, Jacobson T, Broberg C. Comparison of left and right atrial volume by echocardiography versus cardiac magnetic resonance imaging using the area-length method. *Am J Cardiol* 2010;**106**:1345–50.
35. Kebed K, Kruse E, Addetia K, Ciszek B, Thykattil M, Guile B *et al.* Atrial-focused views improve the accuracy of two-dimensional echocardiographic measurements of the left and right atrial volumes: a contribution to the increase in normal values in the guidelines update. *Int J Cardiovasc Imaging* 2017;**33**:209–18.
36. Badano LP, Kolias TJ, Muraru D, Abraham TP, Aurigemma G, Edvardsen T *et al.*; Industry representatives. Standardization of left atrial, right ventricular, and right atrial deformation imaging using two-dimensional speckle tracking echocardiography: a consensus document of the EACVI/ASE/Industry Task Force to standardize deformation imaging. *Eur Heart J Cardiovasc Imaging* 2018;**19**:591–600.
37. Badano LP, Miglioranza MH, Mihaila S, Peluso D, Xhaxho J, Marra MP *et al.* Left atrial volumes and function by three-dimensional echocardiography: reference values, accuracy, reproducibility, and comparison with two-dimensional echocardiographic measurements. *Circ Cardiovasc Imaging* 2016;**9**:e004229.
38. Li W, Wan K, Han Y, Liu H, Cheng W, Sun J *et al.* Reference value of left and right atrial size and phasic function by SSFP CMR at 3.0 T in healthy Chinese adults. *Sci Rep* 2017;**7**:3196.
39. Maceira AM, Cosin-Sales J, Roughton M, Prasad SK, Pennell DJ. Reference right atrial dimensions and volume estimation by steady state free precession cardiovascular magnetic resonance. *J Cardiovasc Magn Reson* 2013;**15**:29.
40. Le Ven F, Bibeau K, De Larochelliere E, Tizon-Marcos H, Deneault-Bissonnette S, Pibarot P *et al.* Cardiac morphology and function reference values derived from a large subset of healthy young Caucasian adults by magnetic resonance imaging. *Eur Heart J Cardiovasc Imaging* 2016;**17**:981–90.
41. Sievers B, Addo M, Breuckmann F, Barkhausen J, Erbel R. Reference right atrial function determined by steady-state free precession cardiovascular magnetic resonance. *J Cardiovasc Magn Reson* 2007;**9**:807–14.
42. Kawel-Boehm N, Hetzel SJ, Ambale-Venkatesh B, Captur G, Francois CJ, Jerosch-Herold M *et al.* Reference ranges ("normal values") for cardiovascular magnetic resonance (CMR) in adults and children: 2020 update. *J Cardiovasc Magn Reson* 2020;**22**:87.
43. Wehrum T, Lodemann T, Hagenlocher P, Stuplich J, Ngo BTT, Grundmann S *et al.* Age-related changes of right atrial morphology and inflow pattern assessed using 4D flow cardiovascular magnetic resonance: results of a population-based study. *J Cardiovasc Magn Reson* 2018;**20**:38.
44. Lin FY, Devereux RB, Roman MJ, Meng J, Jow VM, Jacobs A *et al.* Cardiac chamber volumes, function, and mass as determined by 64-multidetector row computed tomography: mean values among healthy adults free of hypertension and obesity. *JACC Cardiovasc Imaging* 2008;**1**:782–6.
45. Takahashi A, Funabashi N, Kataoka A, Yajima R, Takahashi M, Uehara M *et al.* Quantitative evaluation of right atrial volume and right atrial emptying fraction by 320-slice computed tomography compared with three-dimensional echocardiography. *Int J Cardiol* 2011;**146**:96–9.
46. Rheinheimer S, Reh C, Figiel J, Mahnken AH. Assessment of right atrium volume by conventional CT or MR techniques: which modality resembles in vivo reality? *Eur J Radiol* 2016;**85**:1040–4.
47. Chen YC, Voskoboinik A, Gerche A, Marwick TH, McMullen JR. Prevention of pathological atrial remodeling and atrial fibrillation: JACC state-of-the-art review. *J Am Coll Cardiol* 2021;**77**:2846–64.
48. Delgado V, Di Biase L, Leung M, Romero J, Tops LF, Casadei B *et al.* Structure and function of the left atrium and left atrial appendage: AF and stroke implications. *J Am Coll Cardiol* 2017;**70**:3157–72.
49. Goette A, Kalman JM, Aguinaga L, Akar J, Cabrera JA, Chen SA *et al.*; Review coordinator: Alena Shantsila (UK). EHRA/HRS/APHRS/SOLAECE expert consensus on atrial cardiomyopathies: definition, characterisation, and clinical implication. *J Arrhythm* 2016;**32**:247–78.
50. Shen MJ, Arora R, Jalife J. Atrial myopathy. *JACC Basic Transl Sci* 2019;**4**:640–54.
51. Azemi T, Rabdiya VM, Ayirala SR, McCullough LD, Silverman DI. Left atrial strain is reduced in patients with atrial fibrillation, stroke or TIA, and low risk CHADS(2) scores. *J Am Soc Echocardiogr* 2012;**25**:1327–32.
52. Leung M, van Rosendael PJ, Abou R, Ajmone Marsan N, Leung DY, Delgado V *et al.* Left atrial function to identify patients with atrial fibrillation at high risk of stroke: new insights from a large registry. *Eur Heart J* 2018;**39**:1416–25.
53. Obokata M, Negishi K, Kurosawa K, Tateno R, Tange S, Arai M *et al.* Left atrial strain provides incremental value for embolism risk stratification over CHA(2)DS(2)-VASc score and indicates prognostic impact in patients with atrial fibrillation. *J Am Soc Echocardiogr* 2014;**27**:709–16.e4.

54. Shih JY, Tsai WC, Huang YY, Liu YW, Lin CC, Huang YS *et al.* Association of decreased left atrial strain and strain rate with stroke in chronic atrial fibrillation. *J Am Soc Echocardiogr* 2011;**24**:513–9.
55. Xie E, Yu R, Ambale-Venkatesh B, Bakhshi H, Heckbert SR, Soliman EZ *et al.* Association of right atrial structure with incident atrial fibrillation: a longitudinal cohort cardiovascular magnetic resonance study from the Multi-Ethnic Study of Atherosclerosis (MESA). *J Cardiovasc Magn Reson* 2020;**22**:36.
56. Muller H, Noble S, Keller PF, Sigaud P, Gentil P, Lerch R *et al.* Biatrial anatomical reverse remodelling after radiofrequency catheter ablation for atrial fibrillation: evidence from real-time three-dimensional echocardiography. *Europace* 2008;**10**:1073–8.
57. Soulat-Dufour L, Lang S, Ederhy S, Ancedy Y, Beraud AS, Adavane-Scheuble S *et al.* Biatrial remodelling in atrial fibrillation: a three-dimensional and strain echocardiography insight. *Arch Cardiovasc Dis* 2019;**112**:585–93.
58. Sugumar H, Prabhu S, Voskoboinik A, Young S, Gutman SJ, Wong GR *et al.* Atrial remodeling following catheter ablation for atrial fibrillation-mediated cardiomyopathy: long-term follow-up of CAMERA-MRI study. *JACC Clin Electrophysiol* 2019;**5**:681–8.
59. Therkelsen SK, Groenning BA, Svendsen JH, Jensen GB. Atrial and ventricular volume and function evaluated by magnetic resonance imaging in patients with persistent atrial fibrillation before and after cardioversion. *Am J Cardiol* 2006;**97**:1213–9.
60. Hubert A, Galand V, Donal E, Pavin D, Galli E, Martins RP *et al.* Atrial function is altered in lone paroxysmal atrial fibrillation in male endurance veteran athletes. *Eur Heart J Cardiovasc Imaging* 2018;**19**:145–53.
61. Guasch E, Benito B, Qi X, Cifelli C, Naud P, Shi Y *et al.* Atrial fibrillation promotion by endurance exercise: demonstration and mechanistic exploration in an animal model. *J Am Coll Cardiol* 2013;**62**:68–77.
62. Hiram R, Naud P, Xiong F, Al-u'datt D, Algalarrondo V, Sirois MG *et al.* Right atrial mechanisms of atrial fibrillation in a rat model of right heart disease. *J Am Coll Cardiol* 2019;**74**:1332–47.
63. Hasebe H, Yoshida K, Iida M, Hatano N, Muramatsu T, Aonuma K. Right-to-left frequency gradient during atrial fibrillation initiated by right atrial ectopies and its augmentation by adenosine triphosphate: implications of right atrial fibrillation. *Heart Rhythm* 2016;**13**:354–63.
64. Hasebe H, Yoshida K, Iida M, Hatano N, Muramatsu T, Nogami A *et al.* Differences in the structural characteristics and distribution of epicardial adipose tissue between left and right atrial fibrillation. *Europace* 2018;**20**:435–42.
65. Gu J, Liu X, Tan H, Zhou L, Jiang W, Wang Y *et al.* Impact of chronic obstructive pulmonary disease on procedural outcomes and quality of life in patients with atrial fibrillation undergoing catheter ablation. *J Cardiovasc Electrophysiol* 2013;**24**:148–54.
66. Hayashi T, Fukamizu S, Hojo R, Komiyama K, Tanabe Y, Tejima T *et al.* Prevalence and electrophysiological characteristics of typical atrial flutter in patients with atrial fibrillation and chronic obstructive pulmonary disease. *Europace* 2013;**15**:1777–83.
67. Roh SY, Choi JI, Lee JY, Kwak JJ, Park JS, Kim JB *et al.* Catheter ablation of atrial fibrillation in patients with chronic lung disease. *Circ Arrhythm Electrophysiol* 2011;**4**:815–22.
68. Hiram R, Xiong F, Naud P, Xiao J, Sirois M, Tanguay JF *et al.* The inflammation-resolution promoting molecule resolvin-D1 prevents atrial proarrhythmic remodelling in experimental right heart disease. *Cardiovasc Res* 2021;**117**:1776–89.
69. Li N, Csepe TA, Hansen BJ, Sul LV, Kalyanasundaram A, Zakharkin SO *et al.* Adenosine-induced atrial fibrillation: localized reentrant drivers in lateral right atria due to heterogeneous expression of adenosine A1 receptors and GIRK4 subunits in the human heart. *Circulation* 2016;**134**:486–98.
70. Kaireviciute D, Blann AD, Balakrishnan B, Lane DA, Patel JV, Uzdavinys G *et al.* Characterisation and validity of inflammatory biomarkers in the prediction of post-operative atrial fibrillation in coronary artery disease patients. *Thromb Haemost* 2010;**104**:122–7.
71. Kim YM, Guzik TJ, Zhang YH, Zhang MH, Kattach H, Ratnatunga C *et al.* A myocardial Nox2 containing NAD(P)H oxidase contributes to oxidative stress in human atrial fibrillation. *Circ Res* 2005;**97**:629–36.
72. Neef S, Dybkova N, Sossalla S, Ort KR, Fluschnik N, Neumann K *et al.* CaMKII-dependent diastolic SR Ca2+ leak and elevated diastolic Ca2+ levels in right atrial myocardium of patients with atrial fibrillation. *Circ Res* 2010;**106**:1134–44.
73. Qu YC, Du YM, Wu SL, Chen QX, Wu HL, Zhou SF. Activated nuclear factor-kappaB and increased tumor necrosis factor-alpha in atrial tissue of atrial fibrillation. *Scand Cardiovasc J* 2009;**43**:292–7.
74. Schuster A, Backhaus SJ, Stiermaier T, Navarra JL, Uhlig J, Rommel KP *et al.* Impact of right atrial physiology on heart failure and adverse events after myocardial infarction. *J Clin Med* 2020;**9**:210.
75. Sanz J, Sanchez-Quintana D, Bossone E, Bogaard HJ, Naeije R. Anatomy, function, and dysfunction of the right ventricle: JACC state-of-the-art review. *J Am Coll Cardiol* 2019;**73**:1463–82.
76. Hiram R, Provencher S. Pulmonary disease, pulmonary hypertension and atrial fibrillation. *Card Electrophysiol Clin* 2021;**13**:141–53.
77. Rottlaender D, Motloch LJ, Schmidt D, Reda S, Larbig R, Wolny M *et al.* Clinical impact of atrial fibrillation in patients with pulmonary hypertension. *PLoS One* 2012;**7**:e33902.
78. Cogswell R, Pritzker M, De Marco T. Performance of the REVEAL pulmonary arterial hypertension prediction model using non-invasive and routinely measured parameters. *J Heart Lung Transplant* 2014;**33**:382–7.
79. Raymond RJ, Hinderliter AL, Willis PW, Ralph D, Caldwell EJ, Williams W *et al.* Echocardiographic predictors of adverse outcomes in primary pulmonary hypertension. *J Am Coll Cardiol* 2002;**39**:1214–9.
80. Cannillo M, Grosso Marra W, Gili S, D'Ascenzo F, Morello M, Mercante L *et al.* Supraventricular arrhythmias in patients with pulmonary arterial hypertension. *Am J Cardiol* 2015;**116**:1883–9.
81. Xiao X, Han H, Wu C, He Q, Ruan Y, Zhai Y *et al.* Prevalence of atrial fibrillation in hospital encounters with end-stage COPD on home oxygen: national trends in the United States. *Chest* 2019;**155**:918–27.
82. Carter P, Lagan J, Fortune C, Bhatt DL, Vestbo J, Niven R *et al.* Association of cardiovascular disease with respiratory disease. *J Am Coll Cardiol* 2019;**73**:2166–77.
83. Li J, Agarwal SK, Alonso A, Blecker S, Chamberlain AM, London SJ *et al.* Airflow obstruction, lung function, and incidence of atrial fibrillation: the Atherosclerosis Risk in Communities (ARIC) study. *Circulation* 2014;**129**:971–80.
84. Goedemans L, Leung M, van der Bijl P, Abou R, Vo NM, Ajmone Marsan N *et al.* Influence of chronic obstructive pulmonary disease on atrial mechanics by speckle tracking echocardiography in patients with atrial fibrillation. *Am J Cardiol* 2021;**143**:60–6.
85. Gami AS, Pressman G, Caples SM, Kanagala R, Gard JJ, Davison DE *et al.* Association of atrial fibrillation and obstructive sleep apnea. *Circulation* 2004;**110**:364–7.
86. Iwasaki YK, Kato T, Xiong F, Shi YF, Naud P, Maguy A *et al.* Atrial fibrillation promotion with long-term repetitive obstructive sleep apnea in a rat model. *J Am Coll Cardiol* 2014;**64**:2013–23.
87. Cepelis A, Brumpton BM, Malmo V, Laugsand LE, Loennechen JP, Ellekjær H *et al.* Associations of asthma and asthma control with atrial fibrillation risk: results from the Nord-Trondelag Health Study (HUNT). *JAMA Cardiol* 2018;**3**:721–8.
88. Hornestam B, Adiels M, Wai Giang K, Hansson PO, Bjorck L, Rosengren A. Atrial fibrillation and risk of venous thromboembolism: a Swedish Nationwide Registry Study. *Europace* 2021;**23**:1913–1921.
89. Gaynor SL, Maniar HS, Bloch JB, Steendijk P, Moon MR. Right atrial and ventricular adaptation to chronic right ventricular pressure overload. *Circulation* 2005;**112**:1212–8.
90. Ortiz-Leon XA, Posada-Martinez EL, Trejo-Paredes MC, Ivey-Miranda JB, Pereira J, Crandall I *et al.* Understanding tricuspid valve remodelling in atrial fibrillation using three-dimensional echocardiography. *Eur Heart J Cardiovasc Imaging* 2020;**21**:747–55.
91. Muraru D, Caravita S, Guta AC, Mihalcea D, Branzi G, Parati G *et al.* Functional tricuspid regurgitation and atrial fibrillation: which comes first, the chicken or the egg? *CASE (Phila)* 2020;**4**:458–63.
92. Guta AC, Badano LP, Tomaselli M, Mihalcea D, Bartos D, Parati G *et al.* The pathophysiological link between right atrial remodeling and functional tricuspid regurgitation in patients with atrial fibrillation: a three-dimensional echocardiography study. *J Am Soc Echocardiogr* 2021;**34**:585–94.e1.
93. Muraru D, Addetia K, Guta AC, Ochoa-Jimenez RC, Genovese D, Veronesi F *et al.* Right atrial volume is a major determinant of tricuspid annulus area in functional tricuspid regurgitation: a three-dimensional echocardiographic study. *Eur Heart J Cardiovasc Imaging* 2021;**22**:660–9.
94. Addetia K, Maffessanti F, Muraru D, Singh A, Surkova E, Mor-Avi V *et al.* Morphologic analysis of the normal right ventricle using three-dimensional echocardiography-derived curvature indices. *J Am Soc Echocardiogr* 2018;**31**:614–23.
95. Muraru D, Guta AC, Ochoa-Jimenez RC, Bartos D, Aruta P, Mihaila S *et al.* Functional regurgitation of atrioventricular valves and atrial fibrillation: an elusive pathophysiological link deserving further attention. *J Am Soc Echocardiogr* 2020;**33**:42–53.
96. Topilsky Y, Khanna A, Le Tourneau T, Park S, Michelena H, Suri R *et al.* Clinical context and mechanism of functional tricuspid regurgitation in patients with and without pulmonary hypertension. *Circ Cardiovasc Imaging* 2012;**5**:314–23.
97. Fukuda S, Saracino G, Matsumura Y, Daimon M, Tran H, Greenberg NL *et al.* Three-dimensional geometry of the tricuspid annulus in healthy subjects and in patients with functional tricuspid regurgitation: a real-time, 3-dimensional echocardiographic study. *Circulation* 2006;**114**:1492–8.
98. Utsunomiya H, Itabashi Y, Mihara H, Berdejo J, Kobayashi S, Siegel RJ *et al.* Functional tricuspid regurgitation caused by chronic atrial fibrillation: a real-time

3-dimensional transesophageal echocardiography study. *Circ Cardiovasc Imaging* 2017;**10**: e004897.
99. Badano LP, Hahn R, Rodriguez-Zanella H, Araiza Garaygordobil D, Ochoa-Jimenez RC, Muraru D. Morphological assessment of the tricuspid apparatus and grading regurgitation severity in patients with functional tricuspid regurgitation: thinking outside the box. *JACC Cardiovasc Imaging* 2019;**12**:652–64.
100. Ikoma T, Obokata M, Okada K, Harada T, Sorimachi H, Yoshida K *et al.* Impact of right atrial remodeling in heart failure with preserved ejection fraction. *J Card Fail* 2021;**27**:577–84.
101. Vonk Noordegraaf A, Galie N. The role of the right ventricle in pulmonary arterial hypertension. *Eur Respir Rev* 2011;**20**:243–53.
102. Galie N, Humbert M, Vachiery JL, Gibbs S, Lang I, Torbicki A *et al.*; ESC Scientific Document Group. 2015 ESC/ERS Guidelines for the diagnosis and treatment of pulmonary hypertension: the joint task force for the diagnosis and treatment of pulmonary hypertension of the European Society of Cardiology (ESC) and the European Respiratory Society (ERS): Endorsed by: Association for European Paediatric and Congenital Cardiology (AEPC), International Society for Heart and Lung Transplantation (ISHLT). *Eur Heart J* 2016;**37**:67–119.
103. Liu K, Zhang C, Chen B, Li M, Zhang P. Association between right atrial area measured by echocardiography and prognosis among pulmonary arterial hypertension: a systematic review and meta-analysis. *BMJ Open* 2020;**10**:e031316.
104. Bustamante-Labarta M, Perrone S, De La Fuente RL, Stutzbach P, De La Hoz RP, Torino A *et al.* Right atrial size and tricuspid regurgitation severity predict mortality or transplantation in primary pulmonary hypertension. *J Am Soc Echocardiogr* 2002;**15**:1160–4.
105. Cioffi G, de Simone G, Mureddu G, Tarantini L, Stefenelli C. Right atrial size and function in patients with pulmonary hypertension associated with disorders of respiratory system or hypoxemia. *Eur J Echocardiogr* 2007;**8**:322–31.
106. Jenei C, Kadar R, Balogh L, Borbely A, Gyory F, Peter A *et al.* Role of 3D echocardiography-determined atrial volumes in distinguishing between pre-capillary and post-capillary pulmonary hypertension. *ESC Heart Fail* 2021;**8**:3975–3983.
107. Richter MJ, Fortuni F, Wiegand MA, Dalmer A, Vanderpool R, Ghofrani HA *et al.* Association of right atrial conduit phase with right ventricular lusitropic function in pulmonary hypertension. *Int J Cardiovasc Imaging* 2020;**36**:633–42.
108. Querejeta Roca G, Campbell P, Claggett B, Solomon SD, Shah AM. Right atrial function in pulmonary arterial hypertension. *Circ Cardiovasc Imaging* 2015;**8**: e003521.
109. Alenezi F, Mandawat A, Il'Giovine ZJ, Shaw LK, Siddiqui I, Tapson VF *et al.* Clinical utility and prognostic value of right atrial function in pulmonary hypertension. *Circ Cardiovasc Imaging* 2018;**11**:e006984.
110. Leng S, Dong Y, Wu Y, Zhao X, Ruan W, Zhang G *et al.* Impaired cardiovascular magnetic resonance-derived rapid semiautomated right atrial longitudinal strain is associated with decompensated hemodynamics in pulmonary arterial hypertension. *Circ Cardiovasc Imaging* 2019;**12**:e008582.
111. Yamasaki Y, Abe K, Kamitani T, Hosokawa K, Kawakubo M, Sagiyama K *et al.* Balloon pulmonary angioplasty improves right atrial reservoir and conduit functions in chronic thromboembolic pulmonary hypertension. *Eur Heart J Cardiovasc Imaging* 2020;**21**:855–62.
112. Bai Y, Yang J, Liu J, Ning H, Zhang R. Right atrial function for the prediction of prognosis in connective tissue disease-associated pulmonary arterial hypertension: a study with two-dimensional speckle tracking. *Int J Cardiovasc Imaging* 2019;**35**:1637–49.
113. Frank BS, Schafer M, Thomas TM, Ivy DD, Jone PN. Longitudinal assessment of right atrial conduit fraction provides additional insight to predict adverse events in pediatric pulmonary hypertension. *Int J Cardiol* 2021;**329**:242–5.
114. Hasselberg NE, Kagiyama N, Soyama Y, Sugahara M, Goda A, Ryo-Koriyama K *et al.* The prognostic value of right atrial strain imaging in patients with precapillary pulmonary hypertension. *J Am Soc Echocardiogr* 2021;**34**:851–61.e1.

Corrigendum

https://doi.org/10.1093/ehjci/jeac087
Online publish-ahead-of-print 3 May 2022

Corrigendum to: Imaging assessment of the right atrium: anatomy and function

Roberto M. Lang, Matteo Cameli, L. Elif Sade, Francesco F. Faletra, Federico Fortuni, Alexia Rossi, and Laurie Soulat-Dufour

European Heart Journal - Cardiovascular Imaging, jeac011, https://doi.org/10.1093/ehjci/jeac011

In the originally published version of this manuscript, the third author's name was incorrect. The third author's name should read: "L. Elif Sade". This error has been corrected.